Electronic Supplementary Information

Synthesis of Phosphorescent *syn*, *anti*-Isomeric Clamshell Platinum(II) dimers for OLED Applications

Haibo Yao,[†a,c] Lige Qiao,[†a] Lequn Yuan,[a] Xueyin Luan,[a] Yunjun Shen,[a] Yuzhen Zhang,*[a] Liang Zhou,*[b] Hedong Bian*[a]

[a] Key Laboratory of Chemistry and Engineering of Forest Products, State Ethnic Affairs Commission, Guangxi Key Laboratory of Chemistry and Engineering of Forest Products, Guangxi Collaborative Innovation Center for Chemistry and Engineering of Forest Products, School of Chemistry and Chemical Engineering, Guangxi Minzu University, Nanning 530006, Guangxi, China.

E-Mail: zhangyuzhen@gxmzu.edu.cn. gxunchem@163.com

[b] State Key Laboratory of Rare Earth Resource Utilization, Changchun Institute of Applied Chemistry, Chinese Academy of Sciences, Changchun 130022, P. R. China.

E-mail: zhoul@ciac.ac.cn

[c] Engineering Research Center for Industrial Wastewater Treatment and Reuse of Shandong Province, School of Chemical Engineering and Safety, Shandong University of Aeronautics, Binzhou 256603, Shandong, China.

Table of Contents

General Information

Chemicals

All commercially chemicals are directly purchased without further purification. All commercial reagents were purchased from standard suppliers and were used without further purification.

Characterization

Thin-layer chromatography (TLC) was carried out using silica gel 60, F254 with a thickness of 0.25 mm. Column chromatography was performed on silica gel 60 (200-300 mesh).

NMR spectra were recorded on a Bruker AVANCE III 400 spectrometers (^{1}H NMR 400 MHz, ^{13}C NMR 100 MHz) at 25 °C. Data are reported as follows: Chemical shift in ppm, multiplicity (s = singlet, d = doublet, t = triplet, q = quartet, m = multiplet, dd = doublet of doublets, etc.), coupling constant *J* in Hz, integration, and (where applicable) interpretation.

High-resolution MS data were recorded using ThermoFisher Scientific (USA) equipped with an electrospray ionization source (ESI). Accurate mass determination was corrected by calibration using sodium trifluoroacetate clusters as a reference.

Single-crystal X-ray diffraction studies were performed on Bruker D8 Venture (complex **1-*anti*** and **2-*anti***) using Cu radiation, (complex **1-*syn*** and **4**) using Ga radiation, (complex **2-*syn*** and **3**) using Mo radiation. Olex2 was used in the determination of these structures.

UV−vis absorption measurements were carried out on an Agilent's Cary 100 UV−vis spectrophotometer. Emission spectrum, phosphorescence lifetime and quantum yield were measured directly using Edinburgh Instruments model FLS1000.

Cyclic voltammetry measurements were performed using a CHI 760E electrochemical workstation equipped with a glassy carbon working electrode (d = 2 mm), platinum wire counter electrode, Pt counter electrode, and Ag^{+}/Ag reference electrode. ACS reagent grade solvents were used for the measurements, and the solutions were bubbled with nitrogen for 15 min prior to the test. The voltammograms were referenced to the ferrocence-ferrocenium couple measured under the same

conditions.

The theoretical calculations of the Pt (II) were performed using Gaussian 09 program.[1] The geometries of the ground state S_0 were optimized with the density functional theory (DFT) method with the B3LYP function. The 6-31G (d, p) basis set was used for the C, H and N atoms and LanL2DZ basis set was employed for the Pt atoms. Considering the solvent effect, the DCM was taken as the solvent into the polarizable continuum model (PCM) when the optimizations were conducted. The energies of the singlet and triplet excited states were obtained from the time-dependent density functional theory (TD-DFT) calculations. All molecular structures and orbital compositions were analyzed by Multiwfn [2] and visualized by VMD. [3]

All organic materials used in this study were obtained commercially and used as received without further purification except for compounds **1-*anti***, **2-*anti*** and **3**, which were synthesized and purified experimentally. Indium tin oxide (ITO) coated glass (10 Ω sq^{-1}) was used as the anode substrate. Before device preparation, the ITO glass substrate needs to be carefully cleaned with detergent and ultrasound, and finally placed in an oven for drying. All organic layers were deposited in the organic vacuum chamber at a rate of 0.01 nm s^{-1} under vacuum pressure below 3×10^{-6} Pa. LiF and Al were deposited in the metal vacuum chamber at the rates of 0.01 nm s^{-1} and 0.5 nm s^{-1}, respectively, under vacuum pressure below 3×10^{-6} Pa. Current density-voltage-luminance (*J-V-L*) characteristics, EQE, $CIE_{x,y}$, and EL spectra were measured using M6100 OLED IVL test system.

Experimental Section

The primary ligand of 3,6-Di-tert-butyl-9-(pyrimidin-2-yl)-9H-carbazole ($TBPCH_2$) was prepared by following the reported procedure.[4]

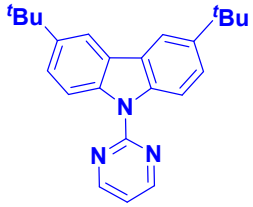

General procedure for synthesizing ligand $TBPCH_2$

2-bromopyrimidine (1.02 g, 6.44 mmol), 3,6-Di-tert-butyl-9H-carbazole (1.50 g, 5.37 mmol), CuCl (4.95mg, 0.06 mmol), *t*-BuOLi (645 mg, 8.06mmol) were added in to a

200 mL one-necked Schlenk flask equipped with a magnetic stirring bar and extracted air for 10 min under the vacuum condition. Then 1-methy-1*H*-imidazole (0.86 mL, 10.7 mmol) and anhydrous and anaerobic toluene solution 50 mL were added into the flask under nitrogen atmosphere. The resulting mixture was bubbled with nitrogen for 10 min and then heated at 130 °C under nitrogen condition for 36 hours. After cooling down to room temperature, the solvent was removed. The residue was extracted with EtOAc. The organic fraction was collected and dried with $MgSO_4$. After the filtration, the solvent was removed and the crude product was purified by silica column chromatography with eluent of EtOAc and *n*-hexane (1:25) to obtain a white powder 1.56 g, 81% yield.

$TBPCH_2$ ^{1}H NMR (400 MHz, $CDCl_3$, δ, ppm): 8.81 – 8.76 (m, 4H), 8.07 (d, *J* = 1.8Hz, 2H), 7.57 – 7.54 (m, 2H), 7.06 (t, *J* = 4.5Hz, 1H), 1.48 (s, 18H). ^{13}C NMR (100 MHz, $CDCl_3$, δ, ppm): 159.22, 157.80, 145.26, 137.51, 125.88, 124.21, 115.92, 115.52, 34.75, 31.87.

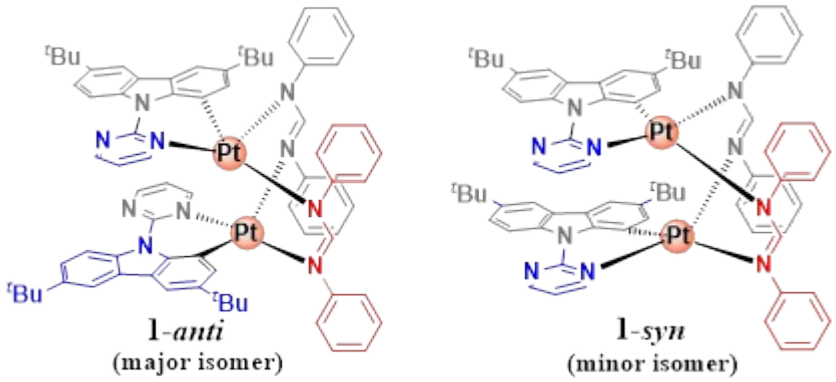

1-*anti* (major isomer) **1-*syn*** (minor isomer)

General procedure for synthesizing complexes 1-*anti* and 1-*syn*.

3,6-Di-tert-butyl-9-(pyrimidin-2-yl)-9H-carbazole ($TBPCH_2$) (536 mg, 1.50 mmol) was added into a 200 mL one-necked Schlenk flask equipped with a magnetic stirring bar and extracted air for 10 min under the vacuum condition. After filling with nitrogen, a solution of K_2PtCl_4 (623 mg, 1.50 mmol) in minor water and 70 mL glacial acetic acid were injected into the flask. The resulting mixture was bubbled with nitrogen for 10 min and then refluxed under nitrogen condition for 24 hours. The mixture was cooled to room temperature and then kept into ice bath for 2 hours, the precipitate was filtered by filtration and washed with water for 3 times and dried with vacuum to generate dichloro-bridged intermediate. These Intermediate products was not purified anymore and used for the next step directly. The dichloro-bridged intermediate (200 mg, 0.170 mmol), N,N'-diphenylformamidine (73.6 mg, 0.370 mmol), aqueous K_2CO_3 solution (4.00 mL, 1.11 mmol) and acetone 50 mL were

antiferred into a Schlenk flask and stirred at reflux condition under nitrogen atmosphere for 24 hrs. After cooling down to room temperature, the solvent was removed. The residue was extracted with DCM. The organic fraction was collected and dried with $MgSO_4$. After the filtration, the solvent was removed and the crude product was purified by silica column chromatography with eluent of CH_2Cl_2 and *n*-hexane. Two complexes was isolated from the crude product: **1-*anti***: Orange solid CH_2Cl_2/hexane (1:10), 49 mg, 19% yield; **1-*syn***: Deep red solid CH_2Cl_2/hexane (1:5), 22 mg, 8.6% yield.

1-*anti* ^{1}H NMR (400 MHz, Methylene Chloride-d2) δ 8.16 (s, 2H), 8.03 (dd, J = 6.2, 2.1 Hz, 2H), 7.85 (dt, J = 4.1, 1.8 Hz, 2H), 7.79 (s, 2H), 7.68 (d, J = 8.8 Hz, 2H), 7.50 (t, J = 9.7 Hz, 8H), 7.29 – 7.21 (m, 8H), 7.04 (t, J = 7.4 Hz, 2H), 6.97 (t, J = 7.2 Hz, 4H), 6.89 (d, J = 8.8 Hz, 2H), 6.81 (t, J = 7.3 Hz, 2H), 5.80 (t, J = 4.8 Hz, 2H), 1.43 (s, 18H), 1.39 (s, 18H). ^{13}C NMR (100 MHz, Methylene Chloride-d_2) δ 161.40, 160.50, 155.02, 152.09, 150.52, 150.41, 145.88, 145.27, 138.33, 136.55, 132.67, 128.62, 128.42, 127.90, 125.49, 123.90, 123.24, 122.81, 122.64, 121.90, 119.00, 115.18, 112.81, 111.27, 34.94, 34.61, 32.15, 31.63, 29.82. HRMS (ESI): *m/z* Calcd. for $C_{74}H_{74}N_{10}Pt_2H$, $[M+H]^+$: 1492.5445. Found: 1492.5387. Elemental analysis: Calc. for $C_{74}H_{74}N_{10}Pt_2 \cdot 1.5H_2O$: C, 58.45%; H, 5.10%; N, 9.21% found: C, 58.81%; H, 4.92%; N, 9.44%.

1-*syn* ^{1}H NMR (400 MHz, Methylene Chloride-d2) δ 8.81 (dd, J = 6.2, 2.3 Hz, 2H), 8.45 – 8.40 (m, 3H), 7.96 – 7.90 (m, 3H), 7.60 – 7.55 (m, 10H), 7.20 (t, J = 8.4, 7.3 Hz, 4H), 7.11 (t, J = 8.5, 7.3 Hz, 4H), 7.05 (dd, J = 8.8, 2.1 Hz, 2H), 7.00 – 6.89 (m, 6H), 6.75 (d, J = 1.9 Hz, 2H), 6.32 (dd, J = 6.2, 4.2 Hz, 2H), 1.41 (s, 18H), 0.99 (s, 18H).^{13}C NMR (100 MHz, Methylene Chloride-d_2) δ 161.76, 161.51, 161.05, 156.28, 151.36, 151.06, 150.73, 145.71, 144.36, 137.82, 136.47, 133.35, 128.91, 128.85, 128.07, 124.56, 123.39, 123.26, 123.18, 122.36, 120.88, 118.71, 115.69, 112.86, 111.03, 107.90, 34.58, 34.35, 31.65, 31.58, 29.82. HRMS (ESI): *m/z* Calcd. for $C_{74}H_{74}N_{10}Pt_2H$, $[M+H]^+$: 1492.5445. Found: 1492.5430. Elemental analysis: Calc. for $C_{74}H_{74}N_{10}Pt_2 \cdot CH_2Cl_2$: C, 57.07%; H, 4.85%; N, 8.87%. Found: C, 57.35%; H, 4.68%; N, 8.52%.

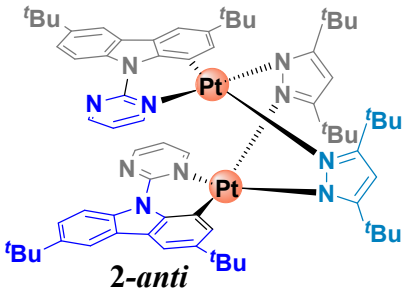

2-*anti*
(major isomer)

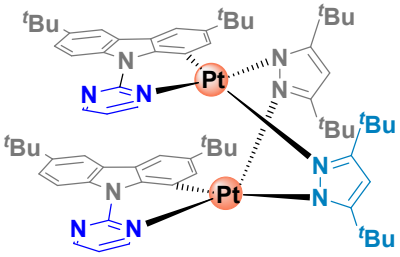

2-*syn*
(minor isomer)

Synthetic procedure for complex 2-*anti* and 2-*syn*. Following the general procedure of preparing complex **1-*anti***. The bridging ligand of 3,5-ditert-butyl-1H-pyrazole[5] (67.4 mg, 0.374 mmol) was used in acetone with K_2CO_3 at 65 °C under N_2 for 24 hrs to prepare complex **2-*anti***: Yellow solid CH_2Cl_2/hexane (1:8) 51 mg, 21% yield; **2-*syn***: Orange solid CH_2Cl_2/hexane (1:3)20 mg, 8.1% yield.

2-*anti* ^{1}H NMR (400 MHz, Methylene Chloride-d_2) δ 10.26 (dd, *J* = 6.0, 2.4 Hz, 2H), 8.68 (d, *J* = 8.8 Hz, 2H), 8.64 (dd, *J* = 4.4, 2.3 Hz, 2H), 8.00 (d, *J* = 2.0 Hz, 2H), 7.59 (d, *J* = 1.8 Hz, 2H), 7.52 (dd, *J* = 8.8, 2.1 Hz, 2H), 6.55 (dd, *J* = 6.0, 4.4 Hz, 2H), 6.06 (s, 2H), 5.98 (d, *J* = 1.9 Hz, 2H), 1.45 (s, 18H), 1.37 (s, 18H), 1.33 (s, 18H), 0.97 (s, 18H).^{13}C NMR (100 MHz, Methylene Chloride-d_2) δ 164.32, 160.99, 159.45, 157.40, 152.70, 146.91, 146.22, 139.53, 137.12, 133.61, 129.34, 123.49, 121.40, 119.37, 116.32, 114.30, 110.78, 101.64, 35.04, 34.85, 32.87, 32.25, 32.15, 31.87, 30.96, 30.08. HRMS (ESI): *m/z* Calcd. for $C_{70}H_{90}N_{10}Pt_2H$, $[M+H]^+$: 1460.6697. Found: 1460.6652. Elemental analysis: Calc. for $C_{70}H_{90}N_{10}Pt_2$: C, 57.52%; H, 6.21%; N, 9.58%. Found: C, 57.88%; H, 6.57%; N, 9.82%.

2-*syn* ^{1}H NMR (400 MHz, Methylene Chloride-d_2) δ 8.72 – 8.62 (m, 4H), 8.47 (d, *J* = 2.1 Hz, 2H), 8.00 (d, *J* = 2.1 Hz, 2H), 7.59 (d, *J* = 1.9 Hz, 2H), 7.52 (dd, *J* = 8.8, 2.1 Hz, 2H), 7.04 (s, 2H), 6.62 (dd, *J* = 6.1, 4.2 Hz, 2H), 6.01 (d, *J* = 27.7 Hz, 2H), 1.46 (s, 18H), 1.20 (d, *J* = 6.5 Hz, 36H), 1.11 (s, 18H). ^{13}C NMR (100 MHz, Methylene Chloride-d_2) δ 161.78, 160.85, 159.61, 156.92, 152.61, 146.79, 145.69, 139.27, 137.10, 134.87, 129.45, 123.10, 121.25, 119.46, 116.14, 114.05, 111.77, 110.03, 101.79, 101.49, 34.79, 34.78, 32.34, 32.16, 32.00, 31.63, 31.36, 31.10. HRMS (ESI): *m/z* Calcd. for $C_{70}H_{90}N_{10}Pt_2H$, $[M+H]^+$: 1460.6697. Found: 1460.6646. Elemental analysis: Calc. for $C_{70}H_{90}N_{10}Pt_2{\cdot}CH_2Cl_2$: C, 55.14%; H, 6.00%; N, 9.06%. Found: C, 54.95%; H, 6.37%; N, 9.25%.

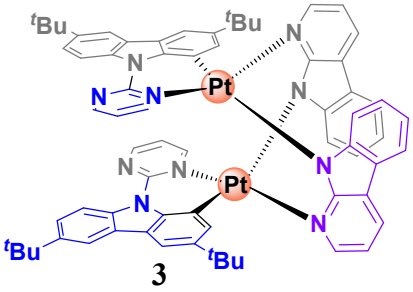

3

Synthetic procedure for complex 3. Following the general procedure. The bridging ligand of 9H-Pyrido[2,3-b]indole (62.9 mg, 0.374 mmol) was used to prepare complex **3**: Yellow solid 72 mg, 30% yield.

3 ^{1}H NMR (400 MHz, Methylene Chloride-d_2) δ 8.78 (dd, *J* = 5.8, 1.4 Hz, 2H), 8.47 (d, *J* = 8.1 Hz, 2H), 8.31 (dd, *J* = 6.2, 2.3 Hz, 2H), 8.17 (dd, *J* = 7.4, 1.4 Hz, 2H), 7.96 (d, *J* = 7.7 Hz, 2H), 7.90 (dd, *J* = 4.2, 2.3 Hz, 2H), 7.81 (d, *J* = 2.0 Hz, 2H), 7.57 (d, *J* = 8.8 Hz, 2H), 7.48 – 7.44 (m, 4H), 7.11 (t, *J* = 7.9, 2H), 6.82 (dd, *J* = 8.8, 2.1 Hz, 2H), 6.75 (dd, *J* = 7.5, 5.9 Hz, 2H), 6.36 (d, *J* = 1.9 Hz, 2H), 5.80 (dd, *J* = 6.2, 4.2 Hz, 2H), 1.44 (s, 18H), 1.02 (s, 18H). ^{13}C NMR (100 MHz, Methylene Chloride-d_2) δ 160.09, 157.48, 155.88, 150.55, 148.41, 147.49, 145.83, 144.88, 137.97, 136.59, 129.59, 127.79, 127.40, 126.45, 123.16, 122.72, 121.85, 120.81, 120.71, 118.85, 118.09, 115.16, 114.51, 112.67, 111.60, 111.24, 34.50, 34.29, 31.54, 31.53, 29.68. HRMS (ESI): *m/z* Calcd. for $C_{70}H_{66}N_{10}Pt_2H$, $[M+H]^+$: 1436.4819. Found: 1436.4767. Elemental analysis: Calc. for $C_{70}H_{66}N_{10}Pt_2 \cdot H_2O$: C, 57.76%; H, 4.71%; N, 9.62%. Found: C, 57.33%; H, 4.66%; N, 9.36%.

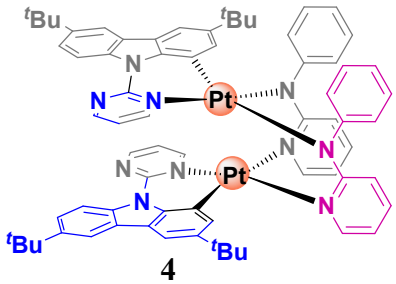

4

Synthetic procedure for complex 4. Following the general procedure. The bridging ligand of 2-anilinopyridine (63.7 mg, 0.374 mmol) was used to prepare complex **4**: Deep red solid 42 mg, 17% yield.

4 ^{1}H NMR (400 MHz, Methylene Chloride-d_2) δ 10.13 (dt, *J* = 6.1, 2.2 Hz, 2H), 8.56 (dd, *J* = 18.4, 8.9 Hz, 2H), 8.41 (dd, *J* = 4.3, 2.3 Hz, 1H), 8.15 – 8.07 (m, 3H), 7.99 (dd, *J* = 9.1, 2.1 Hz, 2H), 7.66 (dd, *J* = 6.3, 1.9 Hz, 2H), 7.55 (d, *J* = 1.9 Hz, 1H), 7.40 (ddd, *J* = 8.8, 8.0, 2.1 Hz, 2H), 7.26 – 7.05 (m, 6H), 7.04 – 6.62 (m, 6H), 6.47 (dd, *J* = 19.9, 9.0 Hz, 2H), 6.22 – 6.07 (m, 2H), 6.04 (td, *J* = 6.5, 1.4 Hz, 1H), 5.98 (dd, *J* = 6.2, 4.3 Hz, 1H),

5.69 (dd, *J* = 6.1, 4.3 Hz, 1H), 1.43 (d, *J* = 1.1 Hz, 18H), 1.41 (s, 9H), 1.30 (s, 9H). ^{13}C NMR (100 MHz, Methylene Chloride-d_2) δ 165.28, 165.14, 164.99, 164.23, 156.82, 155.48, 151.53, 151.49, 151.11, 150.39, 148.48, 146.52, 146.28, 146.17, 145.67, 138.48, 136.69, 136.52, 134.83, 133.99, 131.31, 128.98, 128.58, 128.41, 127.38, 126.65, 125.89, 125.42, 123.37, 122.98, 122.65, 121.59, 121.53, 121.20, 118.90, 118.77, 116.58, 115.65, 115.50, 114.97, 113.00, 112.57, 110.90, 110.83, 109.81, 109.16, 108.64, 34.75, 34.59, 34.56, 34.49, 31.76, 31.68, 31.48, 31.46. HRMS (ESI): *m/z* Calcd. for $C_{70}H_{70}N_{10}Pt_2H$, $[M+H]^+$: 1440.5132. Found: 1440.5092. Elemental analysis: Calc. for $C_{70}H_{70}N_{10}Pt_2 \cdot CH_2Cl_2$: C, 55.87%; H, 4.75%; N, 9.18%. Found: C, 55.71%; H, 4.45%; N, 9.44%.

Table S1. Crystal data and structure refinement for all the complexes

	1-anti	***1-syn***	***2-anti***	***2-syn***	**3**	**4**
CCDC number	2285560	2285561	2285563	2285564	2285565	2285566
Empirical formula	$C_{223}H_{226}N_{30}OPt_6$	$C_{102}H_{106}N_{10}Pt_2$	$C_{70}H_{90}N_{10}Pt_2$	$C_{72}H_{94}N_{10}Pt_2Cl_4$	$C_{71}H_{68}N_{10}Pt_2Cl_2$	$C_{84}H_{126}N_{10}O_{14}Pt_2$
Formula weight	4512.86	1862.14	1461.69	1631.55	1522.43	1890.12
Temperature/K	193.00	213.00	193.00	99.99(10)	193.00	213.00
Crystal system	Monoclinic	Triclinic	Triclinic	Triclinic	Triclinic	Monoclinic
Space group	$P2_1/c$	P-1	P-1	P-1	P-1	$P2_1/n$
a/Å	35.0453(7)	14.5142(12)	12.5525(3)	14.0515(3)	15.0889(11)	16.6809(3)
b/Å	13.1591(2)	17.7460(14)	17.1628(5)	15.3733(3)	16.5091(11)	17.8405(3)
c/Å	46.5467(9)	21.0372(17)	19.2112(6)	18.5567(4)	16.9976(11)	28.5344(5)
α/°	90	65.743(5)	86.287(2)	104.639(2)	116.920(2)	90
β/°	109.6480(10)	88.505(5)	74.490(2)	104.890(2)	100.826(2)	97.0900(10)
γ/°	90	78.217(5)	70.632(2)	101.452(2)	92.785(2)	90
Volume/Å^3	20215.9(7)	4825.9(7)	3761.07(19)	3596.32(14)	3664.7(4)	8426.8(3)
z	4	2	2	2	2	4
ρ_{calc} g/cm^3	1.483	1.281	1.291	1.507	1.380	1.490
μ/mm^{-1}	8.035	3.912	7.173	4.082	3.930	4.561
F(000)	9000.0	1888.0	1472.0	1640.0	1508.0	3872.0
Crystal size/mm^3	0.15 × 0.13 × 0.12	0.07 × 0.07 × 0.05	0.16 × 0.13 × 0.12	0.22 × 0.21 × 0.2	0.15 × 0.13 × 0.12	0.07 × 0.07 × 0.05
2Θ range for data collection/°	5.54 to 133.192	5.422 to 111.034	5.46 to 137.05	3.082 to 58.558	4.236 to 50.054	6.664 to 109.976
Index ranges	-41 ≤ h ≤ 41, -12 ≤ k ≤ 15, -53≤ l ≤ 55	-17 ≤ h ≤ 17, -21 ≤ k ≤ 19, -25 ≤ l ≤ 25	-15 ≤ h ≤ 15, -20 ≤ k ≤ 20, -23 ≤ l ≤ 23	-18 ≤ h ≤ 18, -20 ≤ k ≤ 20, -24 ≤ l ≤ 24	-17 ≤ h ≤ 17, -19 ≤ k ≤ 19, -20 ≤ l ≤ 18	-19 ≤ h ≤ 20 -21 ≤ k ≤ 21, -34 ≤ l ≤ 34
Reflections collected	147527	66341	49578	46510	56449	89782
Independent reflections	35578[$R_{(int)}$=0.0874, R_{sigma} =0.0694]	18298[$R_{(int)}$=0.0737 , R_{sigma} = 0.0752]	13729[R_{int}=0.0497, R_{sigma}=0.0462]	16192[R_{int}=0.0475, R_{sigma}=0.0614]	12797[R_{int}=0.0631, R_{sigma}=0.0486]	15989[R_{int}=0.0631, R_{sigma}=0.0486]
Data/restraints/parameters	35578/6186/2499	18298/82/815	13729/75/824	16192/936/1063	12797/2114/836	15989/37/752
Goodness-of-fit on F^2	1.040	1.300	1.040	1.081	1.058	1.135
Final R indexes [I>=2σ (I)]	R1=0.0426, wR2 = 0.0943	R1 = 0.1011, wR2 = 0.3076	R1 = 0.0568, wR2 = 0.1459	R1 = 0.0409, wR2 = 0.0985	R1 = 0.0343, wR2 = 0.0800	R1 = 0.0510, wR2 = 0.1466
Final R indexes [all data]	R1=0.0615, wR2 = 0.1013	R1 = 0.1162, wR2 = 0.3308	R1 = 0.0637, wR2 = 0.1503	R1 = 0.0610, wR2 = 0.1064	R1 = 0.0445, wR2 = 0.0839	R1=0.0652, wR2 = 0.1540
Largest diff. peak/hole / e Å^{-3}	1.38/-1.05	6.13/-3.23	4.07/-2.35	1.63/-1.79	2.20/-1.13	1.73/-1.61
Flack parameter	n/a	n/a	n/a	n/a	n/a	n/a

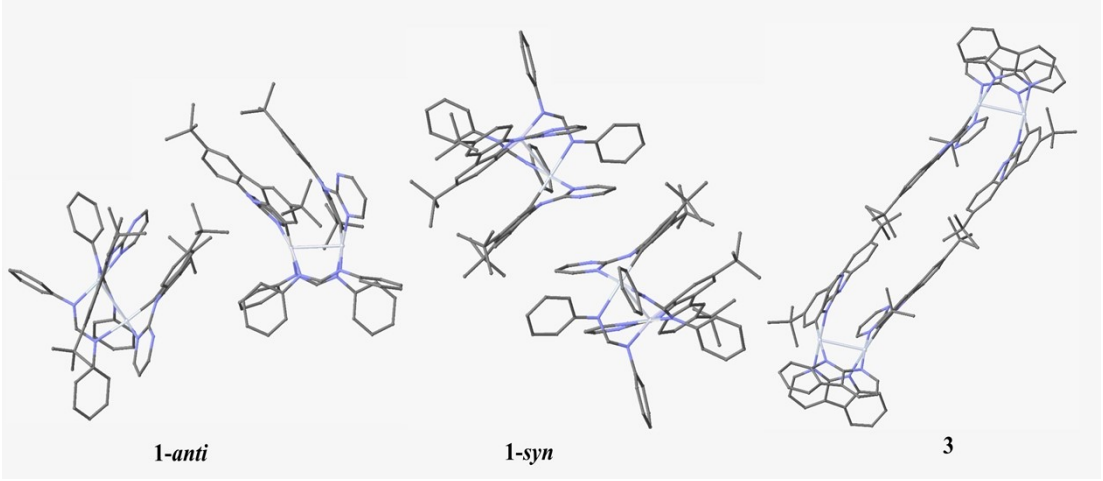

Figure S1. The intermolecular interactions of **1-*anti***, **1-*syn*** and **3** in the crystal structures. Hydrogen atoms are omitted.

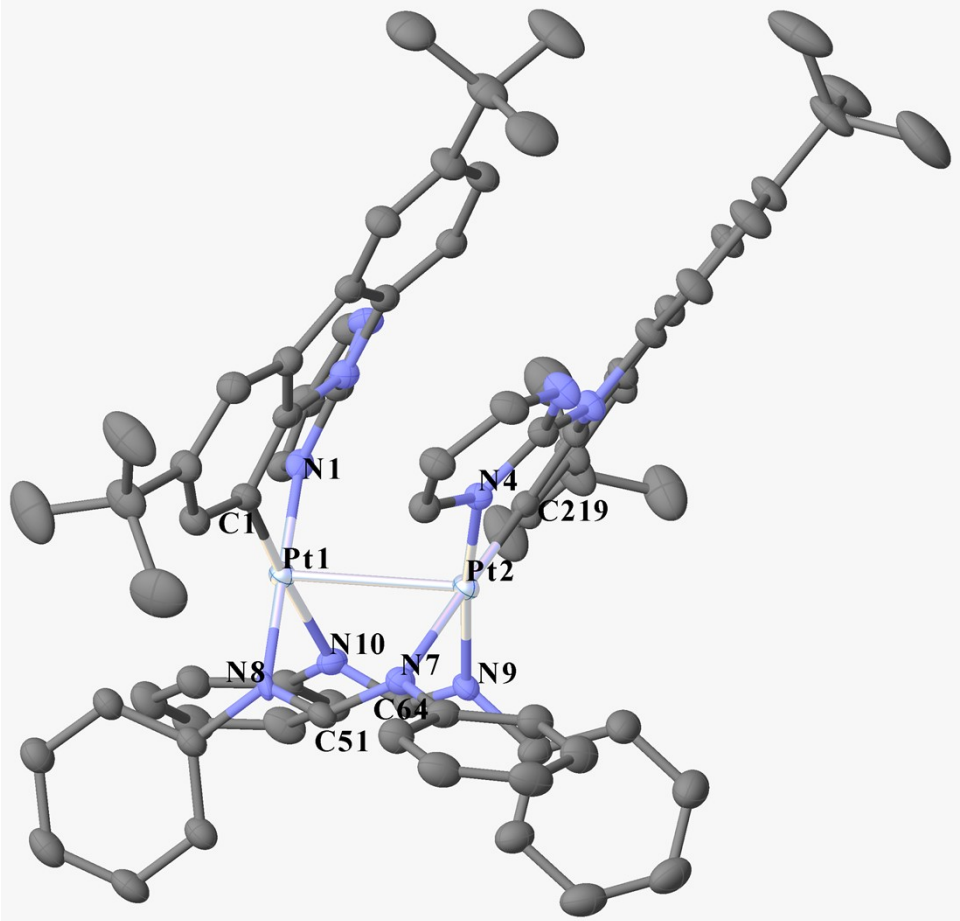

Figure S2. Crystal structure of the complex **1-*anti***. Hydrogen atoms are omitted.

Table S2. Selected Bond Lengths and Angles for **1-*anti***

bond length (Å)			
Pt(1)-C(1)	1.990(7)	Pt(2)-C(219)	1.976(7)
Pt(1)-N(1)	2.020(6)	Pt(2)-N(4)	2.056(5)
Pt(1)-N(8)	2.010(5)	Pt(2)-N(7)	2.144(6)
Pt(1)-N(10)	2.144(5)	Pt(2)-N(9)	2.026(5)
Pt(1)-Pt(2)	2.9442(4)		
bond angle (deg)			
C(1)-Pt(1)-N(1)	89.0(2)	N(4)-Pt(2)-C(219)	90.4(2)
C(1)-Pt(1)-N(8)	92.0(2)	N(4)-Pt(2)-N(7)	91.8(2)
C(1)-Pt(1)-N(10)	174.6(2)	N(4)-Pt(2)-N(9)	172.0(2)
N(10)-Pt(1)-N(8)	85.8(2)	N(9)-Pt(2)-N(7)	85.3(2)
N(10)-Pt(1)-N(1)	93.2(2)	N(9)-Pt(2)-C(219)	92.6(2)
N(1)-Pt(1)-N(8)	179.0(2)	N(7)-Pt(2)-C(219)	177.9(2)

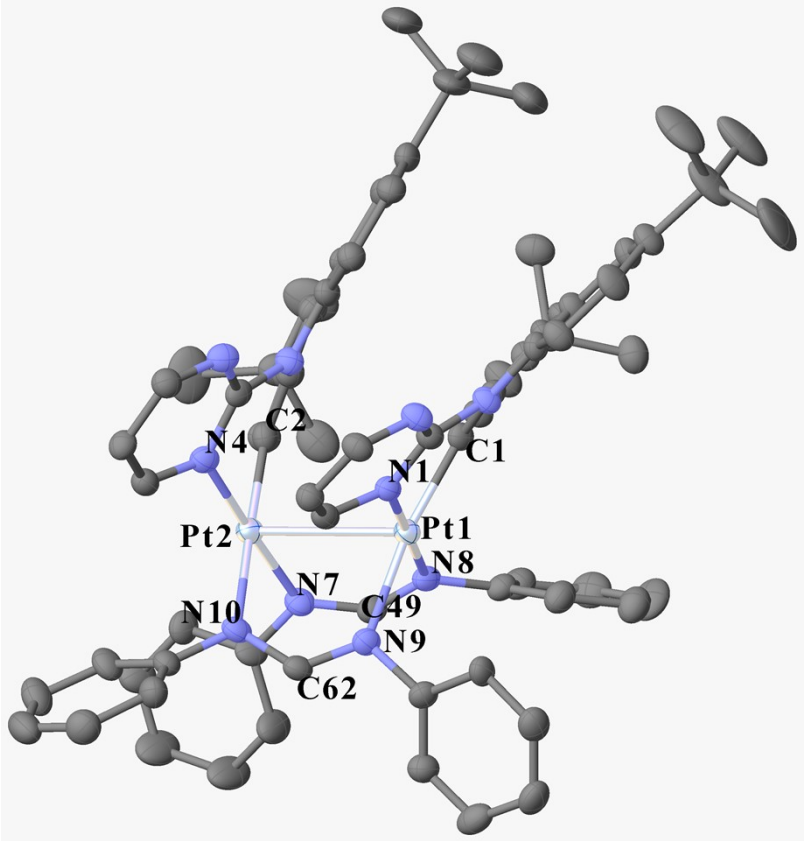

Figure S3. Crystal structure of the complex **1-*syn***. Hydrogen atoms are omitted.

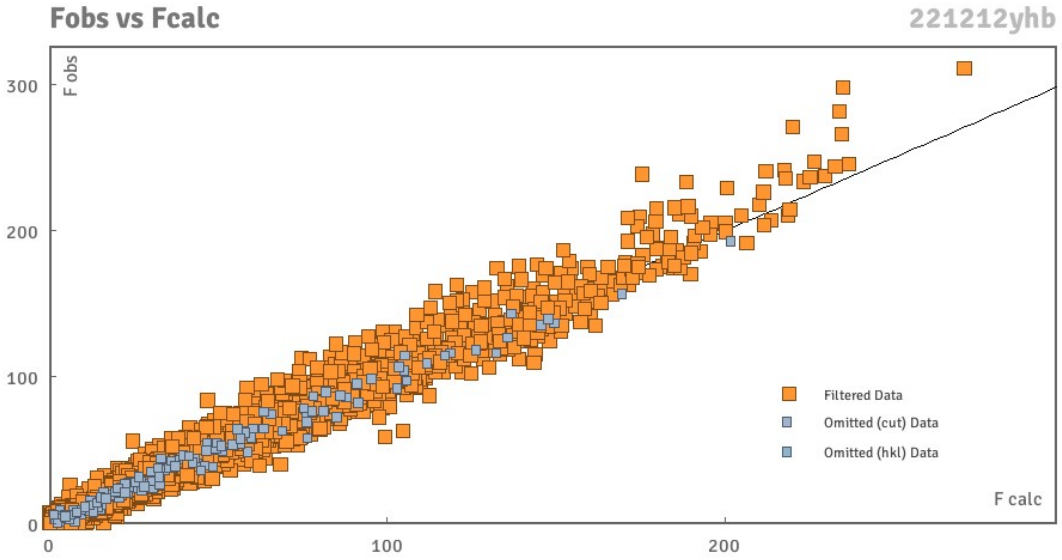

Figure S4. Fobs vs Fcalc plot of complex **1-*syn***.

We have tried many methods with different organic solvents to grow the single crystal for complex **1-*syn***. Unfortunately, we have not obtained one high-quality single crystal suitable for X-ray diffraction. At last, we got needle-like thin crystals with poor quality by slow evaporation of saturated solution of toluene. The poor quality of this single crystal made it difficult to obtain crystal structure data. We used Ga target to test and analysis this single crystal. Usually, the Fobs vs Fcalc of Ga target data exhibit wide spread of the data points, unlike Mo target, which is almost always on the straight-line y=x.

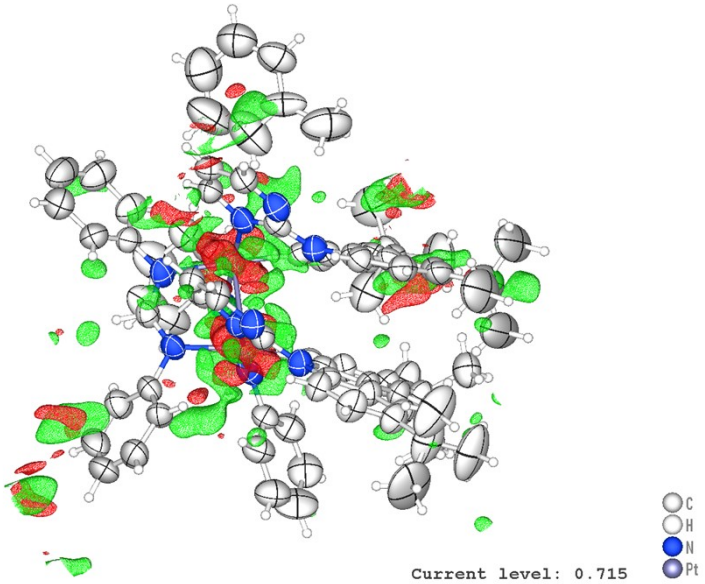

Figure S5. Electron density map of **1-*syn***.

Table S3. Selected Bond Lengths and Angles for **1-*syn***

bond length (Å)			
Pt(1)-C(1)	2.024(9)	Pt(2)-C(2)	2.054(4)
Pt(1)-N(1)	2.039(7)	Pt(2)-N(4)	2.017(8)
Pt(1)-N(8)	2.023(9)	Pt(2)-N(7)	2.042(8)
Pt(1)-N(9)	2.145(7)	Pt(2)-N(10)	2.172(8)
Pt(1)-Pt(2)	2.9763(5)		
bond angle (deg)			
C(1)-Pt(1)-N(1)	90.2(3)	N(4)-Pt(2)-C(2)	86.8(3)
C(1)-Pt(1)-N(8)	91.4(3)	N(4)-Pt(2)-N(7)	177.6(3)
C(1)-Pt(1)-N(9)	171.0(3)	N(4)-Pt(2)-N(10)	93.6(3)
N(9)-Pt(1)-N(8)	86.8(3)	N(10)-Pt(2)-N(7)	86.0(3)
N(9)-Pt(1)-N(1)	91.4(3)	N(7)-Pt(2)-C(2)	93.5(3)
N(1)-Pt(1)-N(8)	178.1(3)	N(7)-Pt(2)-N(4)	177.6.(3)

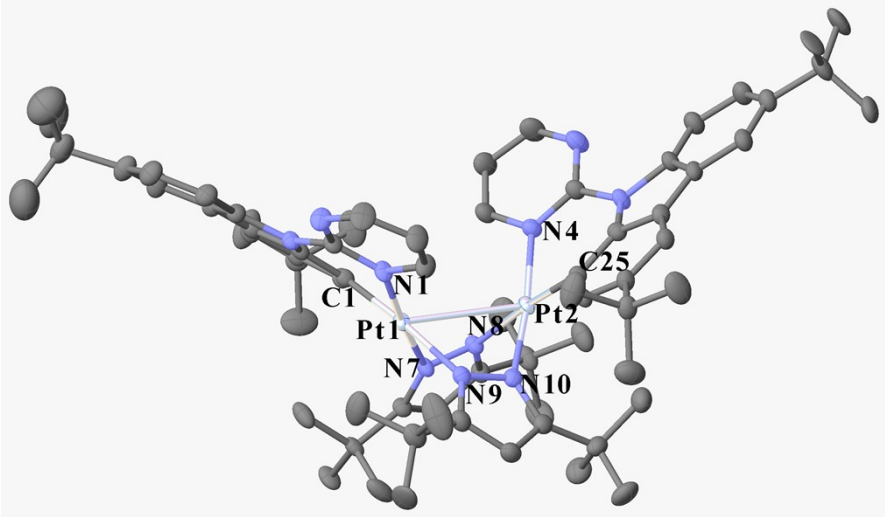

Figure S6. Crystal structure of the complex **2-*anti***. Hydrogen atoms are omitted.

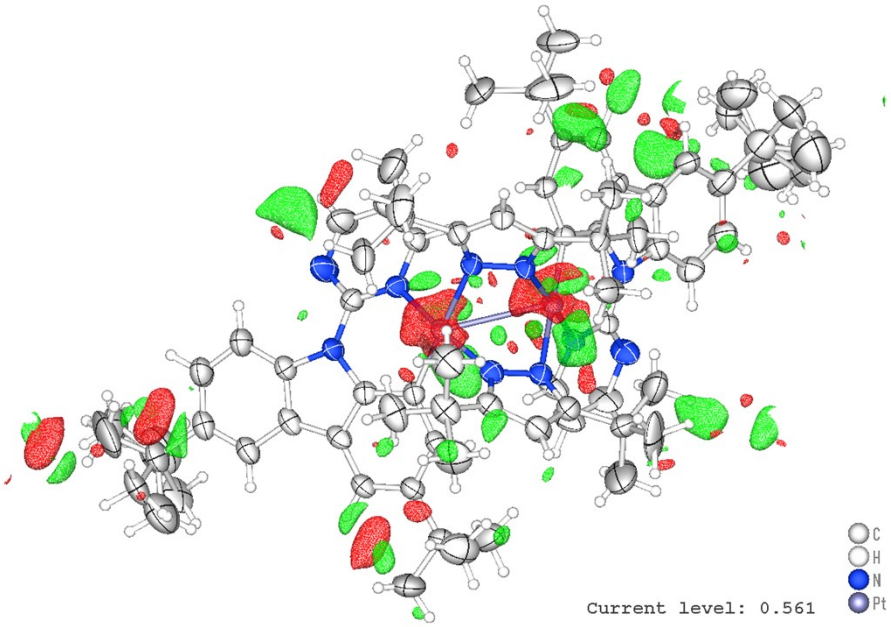

Figure S7. Electron density map of **2-*anti*.**

Because of the low-quality for the crystals, good crystal data was unable to obtain. we have grown single crystals for many times using different solvents and methods, and conducted multiple X-ray single crystal diffraction tests, but not a good one was obtained and this present data is the best one based on the selected crystals. The relatively large residual density is related to heavy Pt atom, which might be by the electronic polarization of the corresponding Pt atom.

Table S4. Selected Bond Lengths and Angles for **2-*anti***

bond length (Å)			
Pt(1)-C(1)	1.987(7)	Pt(2)-C(25)	1.983(7)
Pt(1)-N(1)	2.031(6)	Pt(2)-N(4)	2.047(6)
Pt(1)-N(7)	2.022(6)	Pt(2)-N(8)	2.145(6)
Pt(1)-N(9)	2.158(6)	Pt(2)-N(10)	2.020(7)
Pt(1)-Pt(2)	3.0172(4)		
bond angle (deg)			
C(1)-Pt(1)-N(1)	89.9(3)	N(4)-Pt(2)-C(25)	89.6(3)
C(1)-Pt(1)-N(7)	90.4(3)	N(4)-Pt(2)-N(8)	94.5(2)
C(1)-Pt(1)-N(9)	174.7(3)	N(4)-Pt(2)-N(10)	173.0(3)
N(9)-Pt(1)-N(7)	85.2(2)	N(10)-Pt(2)-N(8)	85.3(2)
N(9)-Pt(1)-N(1)	94.9(2)	N(10)-Pt(2)-C(25)	90.9(3)
N(1)-Pt(1)-N(7)	175.2(2)	N(8)-Pt(2)-C(25)	175.3(3)

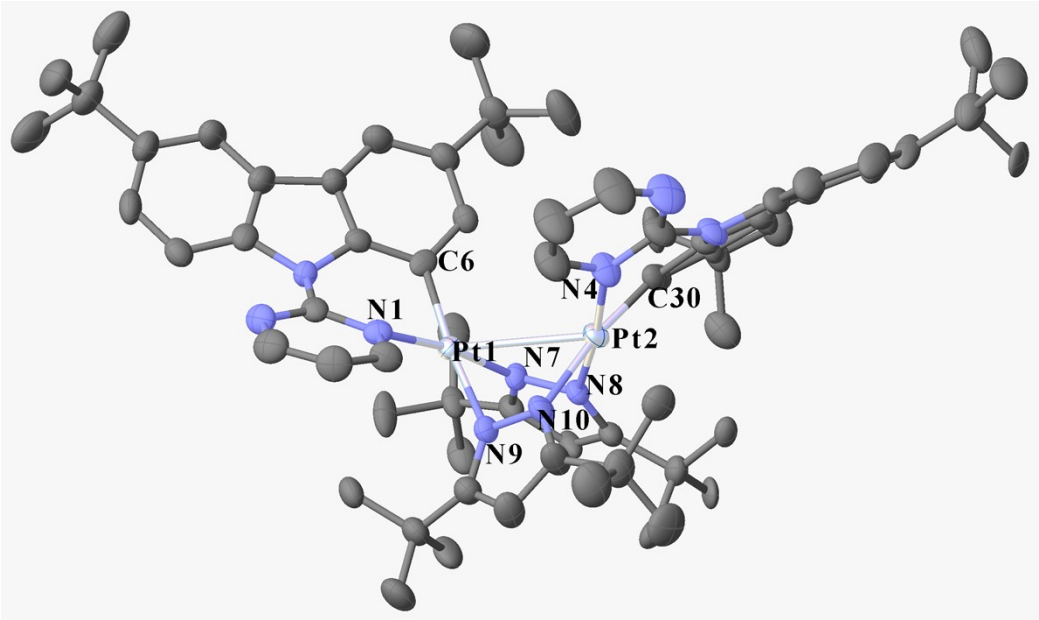

Figure S8. Crystal structure of the complex **2-*syn***. Hydrogen atoms are omitted.

Table S5. Selected Bond Lengths and Angles for **2-*syn***

bond length (Å)			
Pt(1)-C(6)	1.980(5)	Pt(2)-C(30)	1.974(5)
Pt(1)-N(1)	2.038(4)	Pt(2)-N(4)	2.0214)
Pt(1)-N(7)	2.021(4)	Pt(2)-N(8)	2.007(4)
Pt(1)-N(9)	2.116(4)	Pt(2)-N(10)	2.146(4)
Pt(1)-Pt(2)	3.0308(3)		
bond angle (deg)			
C(6)-Pt(1)-N(1)	89.19(18)	N(4)-Pt(2)-C(30)	89.1(2)
C(6)-Pt(1)-N(7)	96.34(18)	N(4)-Pt(2)-N(8)	172.63(16)
C(6)-Pt(1)-N(9)	171.21(17)	N(4)-Pt(2)-N(10)	96.02(18)
N(9)-Pt(1)-N(7)	86.26(16)	N(10)-Pt(2)-N(8)	85.83(16)
N(9)-Pt(1)-N(1)	89.14(16)	N(10)-Pt(2)-C(30)	172.13(17)
N(1)-Pt(1)-N(7)	171.94(15)	N(8)-Pt(2)-C(30)	89.86(19)

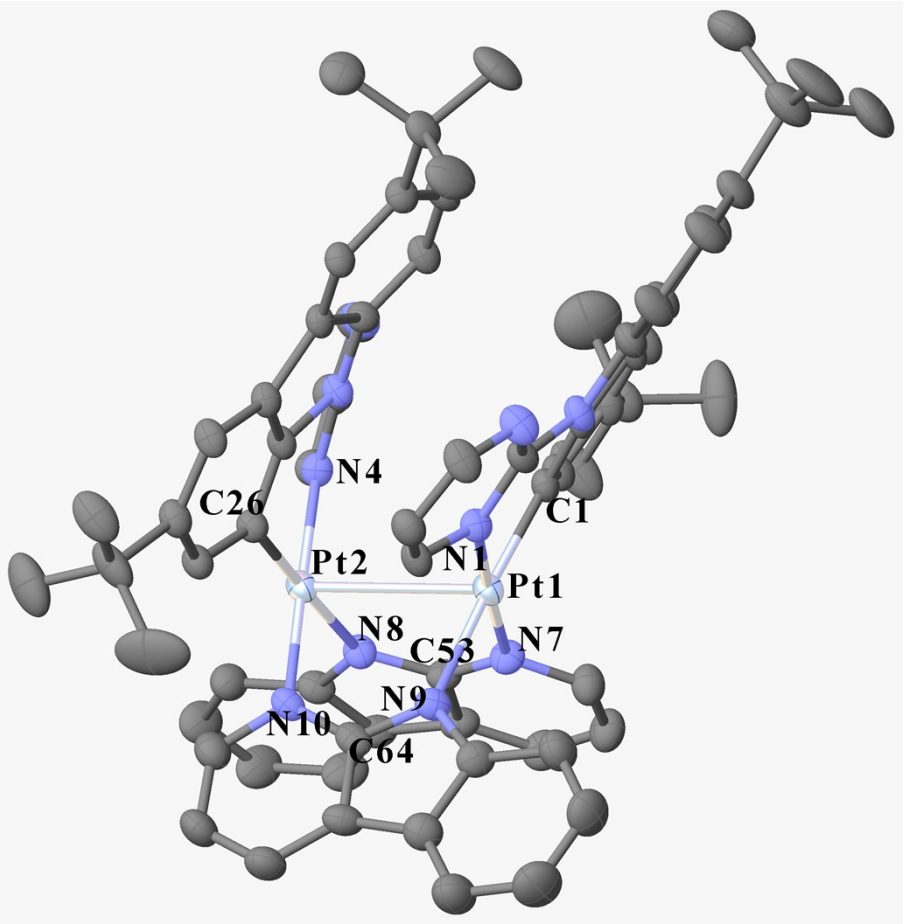

Figure S9. Crystal structure of the complex **3**. Hydrogen atoms are omitted.

Table S6. Selected Bond Lengths and Angles for **3**

bond length (Å)			
Pt(1)-C(1)	1.993(4)	Pt(2)-C(26)	1.997(4)
Pt(1)-N(1)	2.048(4)	Pt(2)-N(4)	2.024(4)
Pt(1)-N(7)	2.031(4)	Pt(2)-N(8)	2.081(4)
Pt(1)-N(9)	2.134(4)	Pt(2)-N(10)	2.014(4)
Pt(1)-Pt(2)	3.0067(3)		
bond angle (deg)			
C(1)-Pt(1)-N(1)	90.64(17)	N(4)-Pt(2)-C(26)	89.64(17)
C(1)-Pt(1)-N(7)	90.09 (17)	N(4)-Pt(2)-N(8)	91.77(15)
C(1)-Pt(1)-N(9)	177.04(17)	N(4)-Pt(2)-N(10)	178.16(14)
N(9)-Pt(1)-N(7)	88.26(15)	N(10)-Pt(2)-N(8)	86.41(15)
N(9)-Pt(1)-N(1)	90.85(15)	N(10)-Pt(2)-C(26)	92.16(17)
N(1)-Pt(1)-N(7)	176.21(16)	N(8)-Pt(2)-C(26)	176.32(18)

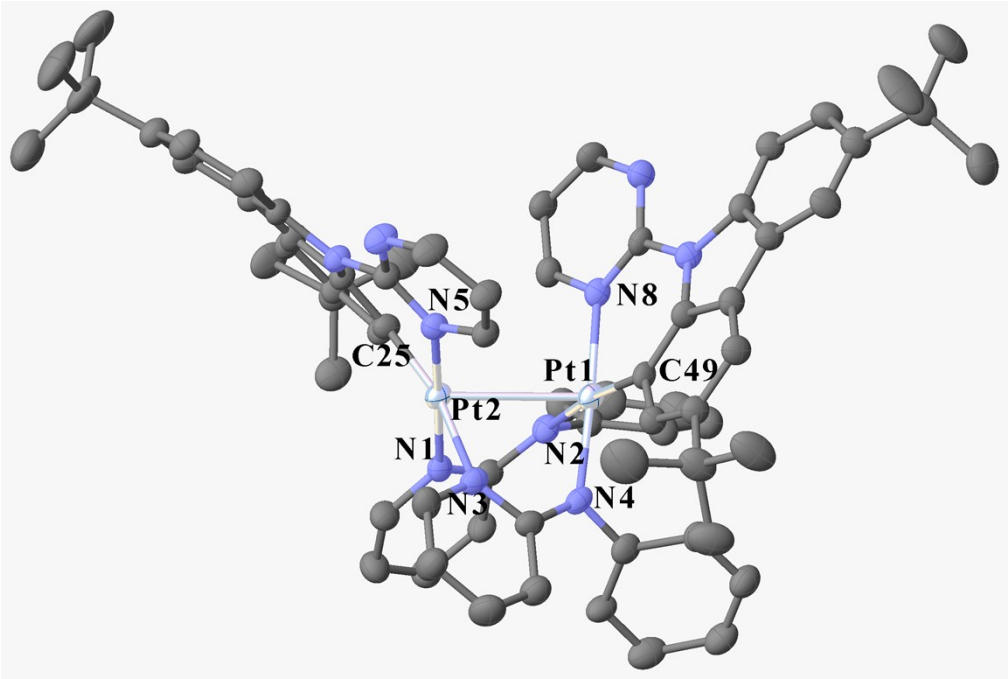

Figure S10. Crystal structure of the complex **4**. Hydrogen atoms are omitted.

Table S7. Selected Bond Lengths and Angles for **4**

bond length (Å)			
Pt(1)-C(49)	1.985(5)	Pt(2)-C(25)	1.988(5)
Pt(1)-N(8)	2.051(4)	Pt(2)-N(1)	2.013(4)
Pt(1)-N(2)	2.163(5)	Pt(2)-N(3)	2.151(4)
Pt(1)-N(4)	2.037(4)	Pt(2)-N(5)	2.040(4)
Pt(1)-Pt(2)	2.9184(3)		
bond angle (deg)			
C(49)-Pt(1)-N(8)	90.31(19)	N(5)-Pt(2)-C(25)	89.9(2)
C(49)-Pt(1)-N(4)	92.13(19)	N(5)-Pt(2)-N(3)	92.53(17)
C(49)-Pt(1)-N(2)	171.79(18)	N(5)-Pt(2)-N(1)	176.95(17)
N(2)-Pt(1)-N(4)	85.00(17)	N(1)-Pt(2)-N(3)	85.24(17)
N(2)-Pt(1)-N(8)	92.84(17)	N(1)-Pt(2)-C(25)	92.9(2)
N(4)-Pt(1)-N(8)	176.84(17)	N(3)-Pt(2)-C(25)	168.3(2)

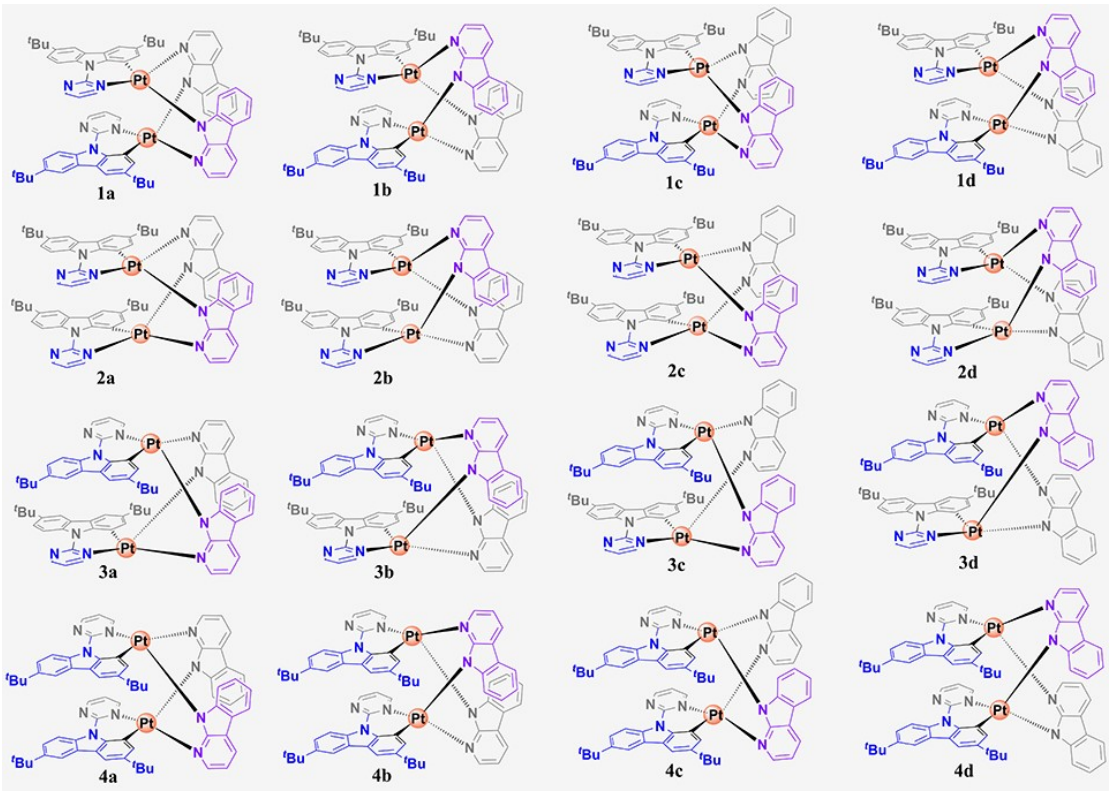

Figure S11. Possible configurations of complex **3**.

Based on the spatial configurations of the primary cyclometallation and bridging ligands, we have made our best to draw 16 possible molecular configurations. Through analysis, we have found that 1a and 3b, 3a and 1b, 1c and 3d, 3c and 1d, 2a and 2b, 2c and 4c are mirror images of each other, respectively; 1c and 1d, 2b and 4b, 2a and 4a, 3c and 3d, 2c and 4d, 4c and 2d are the same. Therefore, theoretically, there will be 10 isomers produced.

Table S8. Frontier orbital energies, distributions, and assignments of all the complexes at the optimized S_0 geometries

	MO	Energy	MO distribution (%)			
		(eV)	d(Pt)	Cz	Py	L[a]
1-*anti*	H-2	-5.53	12.69	10.91	2.00	74.40
	H-1	-5.39	26.05	17.71	3.81	52.44
	H	-5.12	64.25	18.14	3.47	14.15
	L	-1.56	3.94	5.67	88.53	1.87
	L+1	-1.44	3.36	5.70	87.83	3.11
	L+2	-1.05	0.97	40.51	56.50	2.01
1-*syn*	H-2	-5.56	13.37	12.16	2.54	71.93
	H-1	-5.39	27.79	16.83	3.83	51.55
	H	-5.15	58.35	23.52	4.14	13.99
	L	-1.67	3.84	3.56	90.37	2.24
	L+1	-1.53	3.30	4.75	89.61	2.34
	L+2	-1.06	1.18	35.31	61.34	2.17
2 *anti*	H-2	-5.73	36.16	39.65	7.22	16.97
	H-1	-5.64	20.43	61.22	8.95	9.40
	H	-5.35	65.04	23.84	3.92	7.20
	L	-1.62	3.36	4.34	89.91	2.40
	L+1	-1.62	3.34	4.43	89.93	2.30
	L+2	-1.09	1.16	38.44	59.24	1.16
2-*syn*	H-2	-5.72	49.19	28.59	4.97	17.26
	H-1	-5.61	21.26	57.48	8.07	13.18
	H	-5.43	52.39	34.08	5.66	7.87
	L	-1.66	3.48	3.50	90.28	2.74
	L+1	-1.66	3.23	3.69	91.22	1.87
	L+2	-1.10	1.09	34.08	63.32	1.52
3	H-2	-5.66	8.61	6.39	2.22	82.78
	H-1	-5.56	16.95	14.79	3.94	64.32
	H	-5.32	61.12	27.22	5.03	6.64
	L	-1.59	3.94	5.56	88.20	2.30
	L+1	-1.47	3.07	6.21	86.44	4.28
	L+2	-1.24	1.55	1.53	2.55	94.38
4	H-2	-5.30	38.44	13.28	2.52	45.76
	H-1	-5.13	25.43	8.09	1.74	64.74
	H	-5.06	28.51	13.86	2.76	54.87
	L	-1.60	3.62	4.83	89.74	1.82
	L+1	-1.45	3.77	4.97	88.34	2.92
	L+2	-1.07	1.06	38.99	58.50	1.45

[a] L stands for the N^N ligand.

Table S9. Excited state properties of studied complexes calculated at the optimized S_0 geometry by TDDFT

Complex	State	E/eV	λcalc./nm	*f*	Antiition	Coefficient
1-*anti*	S0→S1	2.69	461.5	0.0223	HOMO→LUMO	0.69
					HOMO-1→LUMO	-0.11
	S0→S2	2.80	441.7	0.0184	HOMO→LUMO+1	0.70
	S0→S3	3.09	400.7	0.0479	HOMO-1→LUMO	0.58
					HOMO-1→LUMO+1	0.35
1-*syn*	S0→S1	2.63	471.2	0.0299	HOMO→LUMO	0.68
					HOMO-1→LUMO	0.14
	S0→S2	2.77	447.2	0.0106	HOMO→LUMO+1	0.69
					HOMO-1→LUMO+1	0.12
	S0→S3	3.00	413.0	0.0713	HOMO-1→LUMO	0.63
					HOMO-3→LUMO+1	-0.16
					HOMO-1→LUMO+1	-0.15
					HOMO-1→LUMO	-0.12
2-*anti*	S0→S1	2.86	433.6	0.0128	HOMO→LUMO	0.68
					HOMO→LUMO+1	0.12
	S0→S2	2.86	432.6	0.0082	HOMO→LUMO+1	0.68
					HOMO→LUMO	-0.12
	S0→S3	3.18	390.3	0.0405	HOMO-1→LUMO	0.53
					HOMO-2→LUMO	0.42
					HOMO-1→LUMO+1	0.17
2-*syn*	S0→S1	2.90	427.6	0.0175	HOMO→LUMO+1	0.51
					HOMO→LUMO	0.46
	S0→S2	2.96	419.1	0.0499	HOMO→LUMO	0.48
					HOMO→LUMO+1	-0.44
					HOMO-1→LUMO	0.14
	S0→S3	3.10	400.4	0.0278	HOMO-1→LUMO	0.46
					HOMO-1→LUMO+1	-0.38
					HOMO-2→LUMO	-0.26
3	S0→S1	2.85	434.5	0.0198	HOMO→LUMO	0.69
	S0→S2	2.97	416.8	0.0184	HOMO→LUMO+1	0.70
	S0→S3	3.19	388.2	0.0690	HOMO-1→LUMO	0.59
					HOMO-2→LUMO	-0.28
4	S0→S1	2.67	464.2	0.0174	HOMO→LUMO	0.54
					HOMO-1→LUMO	0.37
					HOMO-2→LUMO	-0.25
	S0→S2	2.79	443.9	0.0286	HOMO→LUMO+1	0.67
					HOMO-2→LUMO+1	-0.21
	S0→S3	2.85	434.7	0.0059	HOMO-1→LUMO+1	0.65
					HOMO-2→LUMO+1	-0.23

Table S10. Excited state properties of studied complexes calculated at the optimized T_1 geometry by TDDFT.

Complex	State	E/eV	λcalc./nm	*f*	Antiition	Coefficient
1-*anti*	T1	1.70	728.9	0	HOMO→LUMO (96.5%)	0.69
	T2	2.41	514.9	0	HOMO-1→LUMO (40.7%)	0.45
					HOMO-3→LUMO (31.2%)	-0.40
					HOMO→LUMO+1 (12.7%)	0.25
1-*syn*	T1	1.43	868.9	0	HOMO→LUMO (98.7%)	0.70
	T2	2.19	565.9	0	HOMO-2→LUMO (63.7%)	0.56
					HOMO-1→LUMO (26.2%)	-0.36
					HOMO-2→LUMO (9.1%)	-0.21
2-*anti*	T1	1.84	673.9	0	HOMO→LUMO (95.4%)	0.69
	T2	2.30	538.6	0	HOMO-1→LUMO (60.0%)	0.54
					HOMO-2→LUMO (29.3%)	-0.38
2-*syn*	T1	1.82	680.0	0	HOMO→LUMO (95.8%)	0.69
	T2	2.24	553.5	0	HOMO-1→LUMO (73.0%)	0.60
					HOMO-2→LUMO (17.2%)	0.29
3	T1	1.89	655.1	0	HOMO→LUMO (96.8%)	0.70
	T2	2.50	495.2	0	HOMO-2→LUMO (42.1%)	0.46
					HOMO-3→LUMO (31.7%)	0.39
					HOMO-4→LUMO (10.7%)	0.23
					HOMO-1→LUMO(5.6%)	0.17
4	T1	1.55	802.0	0	HOMO→LUMO (94.2%)	0.69
	T2	2.20	562.5	0	HOMO-1→LUMO (67.0%)	0.57
					HOMO-2→LUMO (21.8%)	-0.33
					HOMO-3→LUMO (5.7%)	-0.17

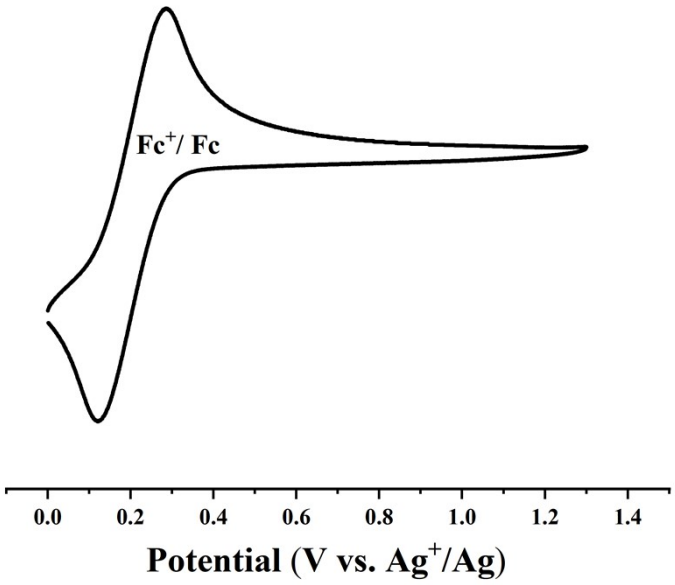

Figure S12. The cyclic voltammograms spectra of ferrocene

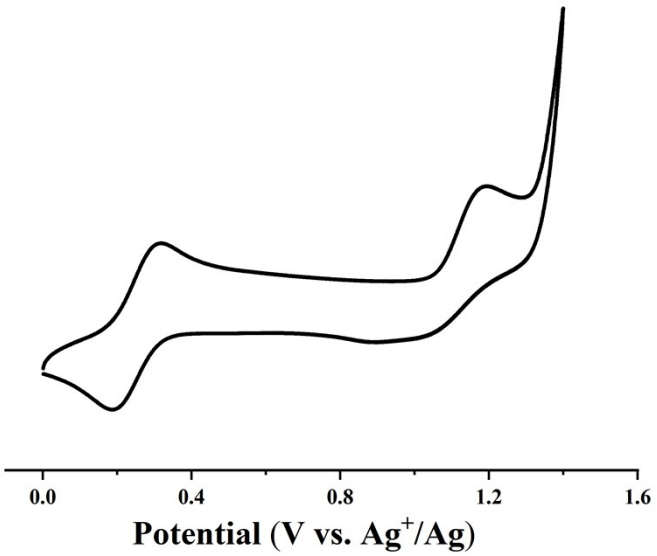

Figure S13. The cyclic voltammograms spectra of **1-*anti***

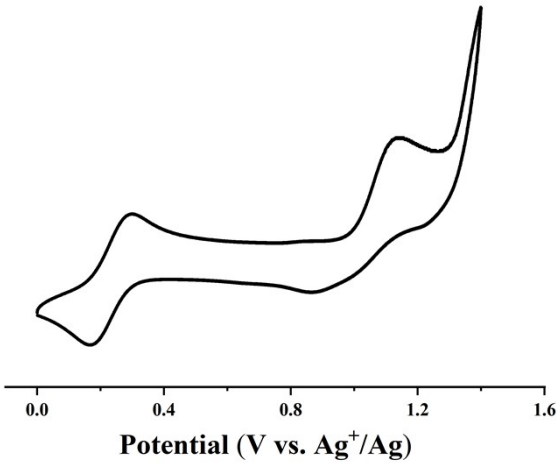

Figure S14. The cyclic voltammograms spectra of **1-*syn***

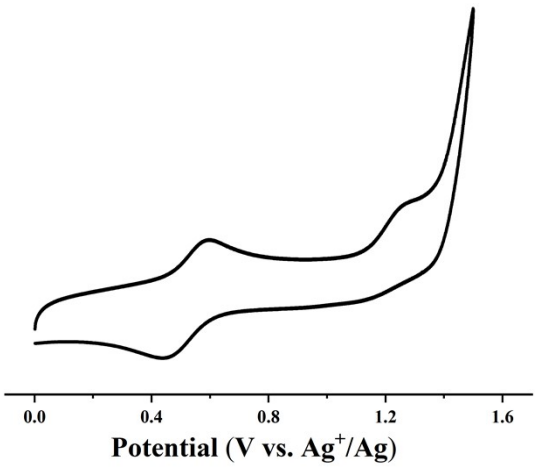

Figure S15. The cyclic voltammograms spectra of **2-*anti***

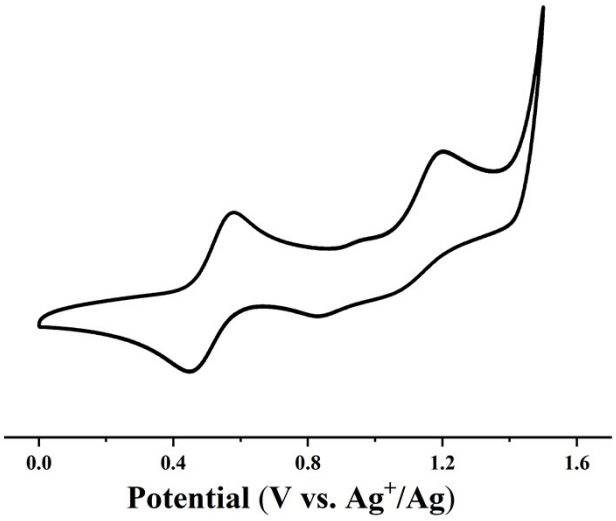

Figure S16. The cyclic voltammograms spectra of **2-*syn***

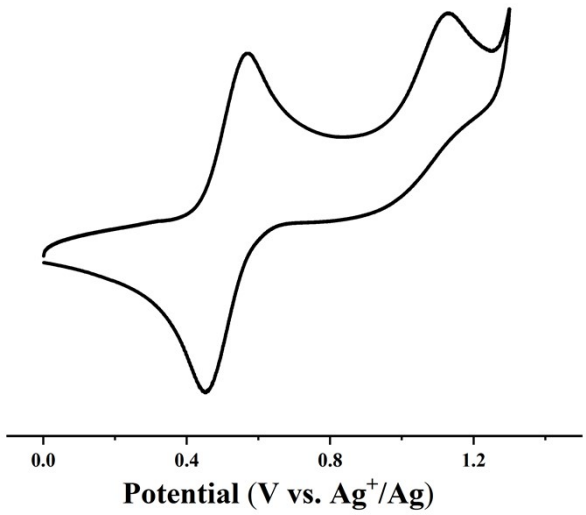

Figure S17. The cyclic voltammograms spectra of **3**

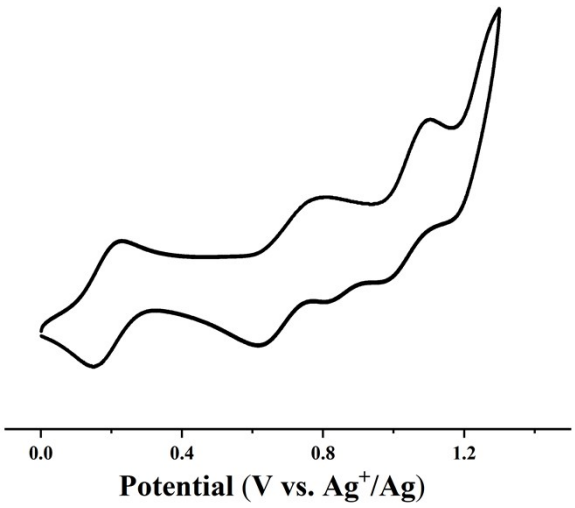

Figure S18. The cyclic voltammograms spectra of **4**

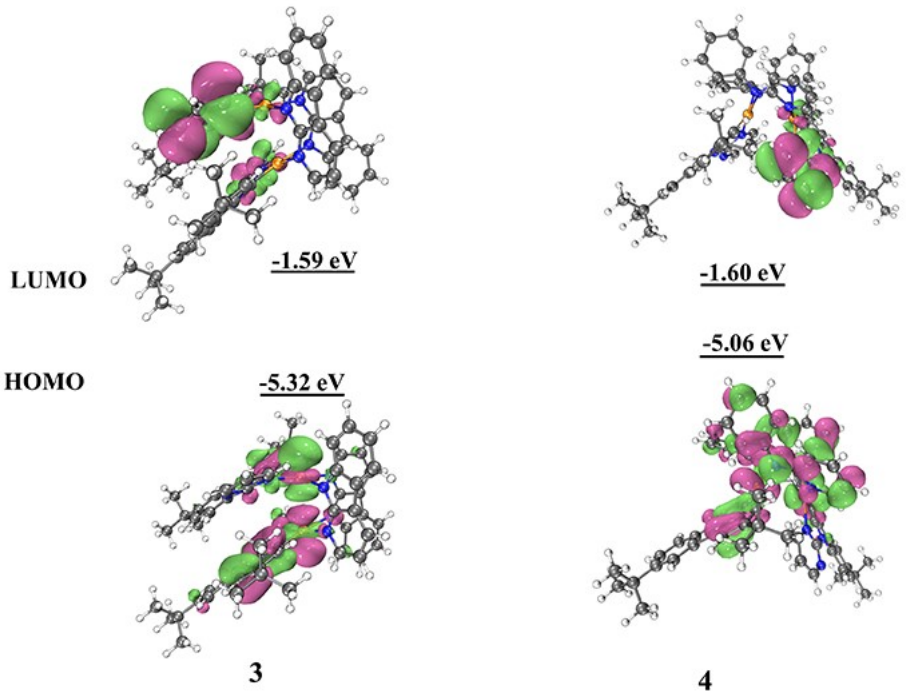

Figure S19. Frontier orbital diagrams for the HOMOs/LUMOs and their energy levels for **3** and **4** calculated in CH_2Cl_2 (isovalue=0.02).

References

1 Gaussian 09, Revision E.01, M. J. Frisch, G. W. Trucks, H. B. Schlegel, G. E. Scuseria, M. A. Robb, J. R. Cheeseman, G. Scalmani, V. Barone, B. Mennucci, G. A. Petersson, H. Nakatsuji, M. Caricato, X. Li, H. P. Hratchian, A. F. Izmaylov, J. Bloino, G. Zheng, J. L. Sonnenberg, M. Hada, M. Ehara, K. Toyota, R. Fukuda, J. Hasegawa, M. Ishida, T. Nakajima, Y. Honda, O. Kitao, H. Nakai, T. Vreven, J. A. Montgomery, Jr., J. E. Peralta, F. Ogliaro, M. Bearpark, J. J. Heyd, E. Brothers, K. N. Kudin, V. N. Staroverov, T. Keith, R. Kobayashi, J. Normand, K. Raghavachari, A. Rendell, J. C. Burant, S. S. Iyengar, J. Tomasi, M. Cossi, N. Rega, J. M. Millam, M. Klene, J. E. Knox, J. B. Cross, V. Bakken, C. Adamo, J. Jaramillo, R. Gomperts, R. E. Stratmann, O. Yazyev, A. J. Austin, R. Cammi, C. Pomelli, J. W. Ochterski, R. L. Martin, K. Morokuma, V. G. Zakrzewski, G. A. Voth, P. Salvador, J. J. Dannenberg, S. Dapprich, A. D. Daniels, O. Farkas, J. B. Foresman, J. V. Ortiz, J. Cioslowski, and D. J. Fox, Gaussian, Inc., Wallingford CT, 2013.

2 T. Lu and F. Chen, *J. Comput. Chem.*, 2012, **33**, 580-592.

3 W. Humphrey, A. Dalke and K. Schulten, *J. Mol. Graph.*, 1996, **14**, 33-38, 27-38.

4 V. P. Reddy, R. Qiu, T. Iwasaki and N. Kambe, *Org. Lett.*, 2013, **15**, 1290-1293.

5 J. L. van Wyk, B. Omondi, D. Appavoo, I. A. Guzei and J. Darkwa, *J. Chem. Res.*, 2012, **8**, 474–477.

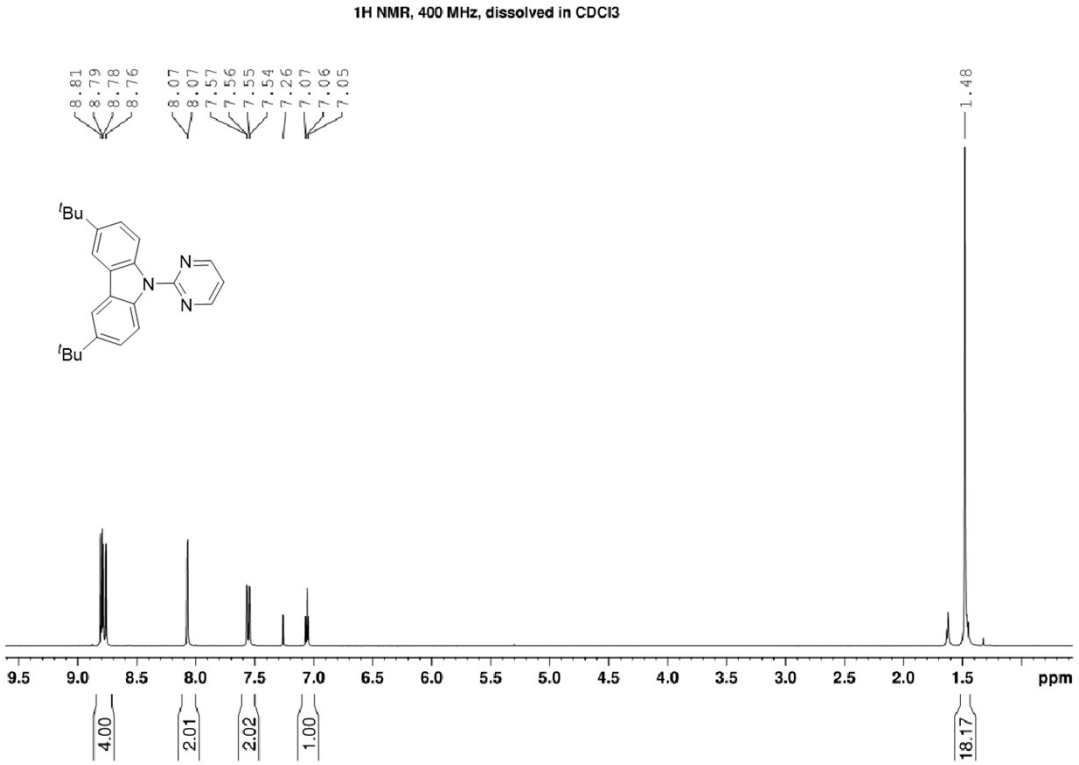

Figure S20. ^{1}H NMR spectrum of **TBPCH$_2$** ($CDCl_3$)

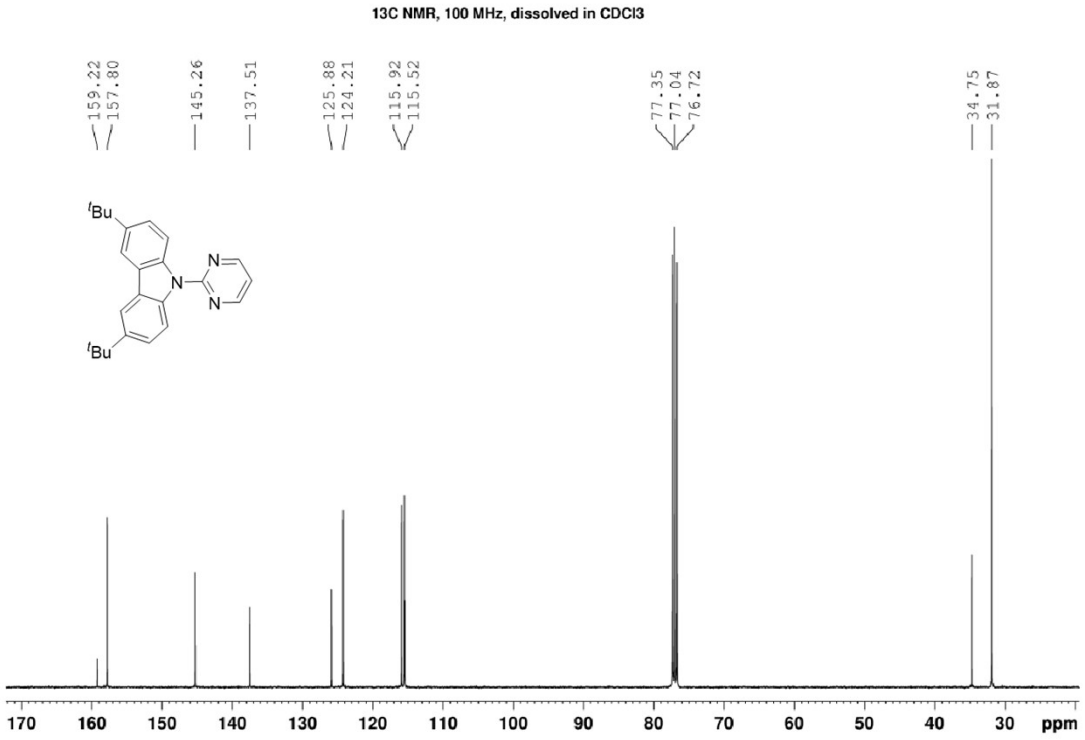

Figure S21. ^{13}C NMR spectrum of **TBPCH$_2$** ($CDCl_3$)

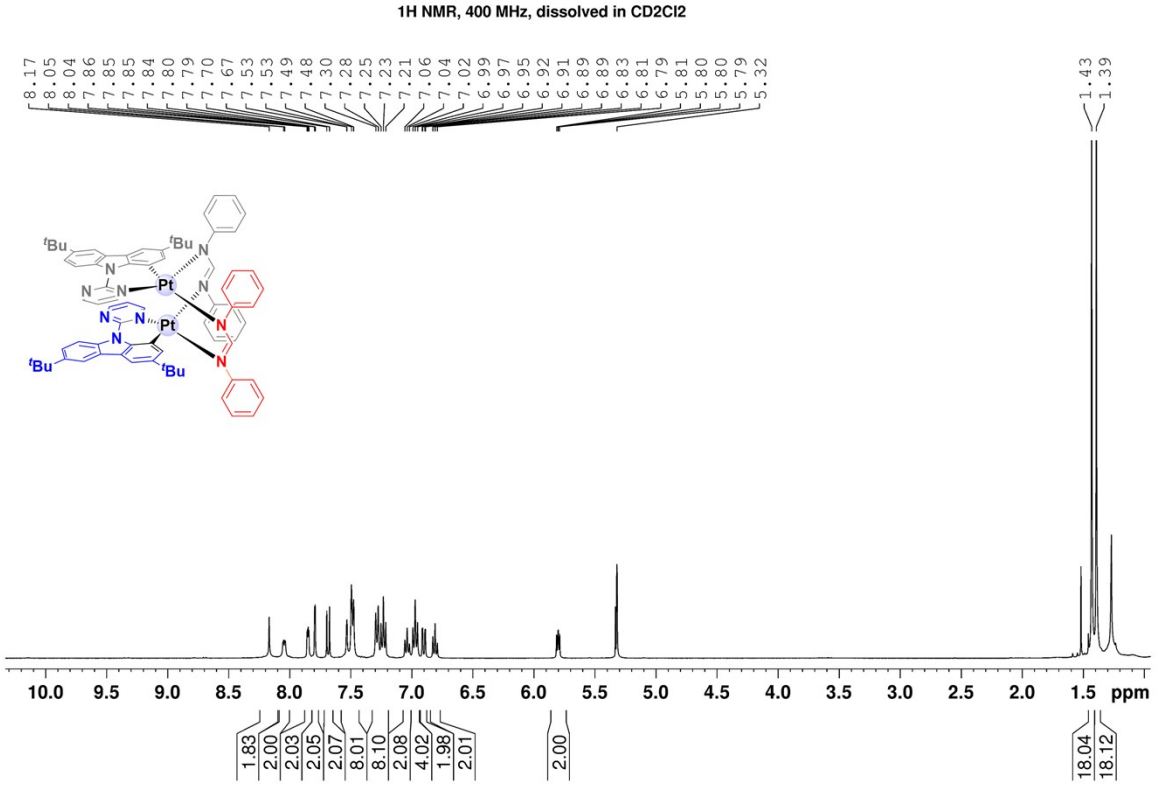

Figure S22. ^{1}H NMR spectrum of **1-*anti*** (CD_2Cl_2)

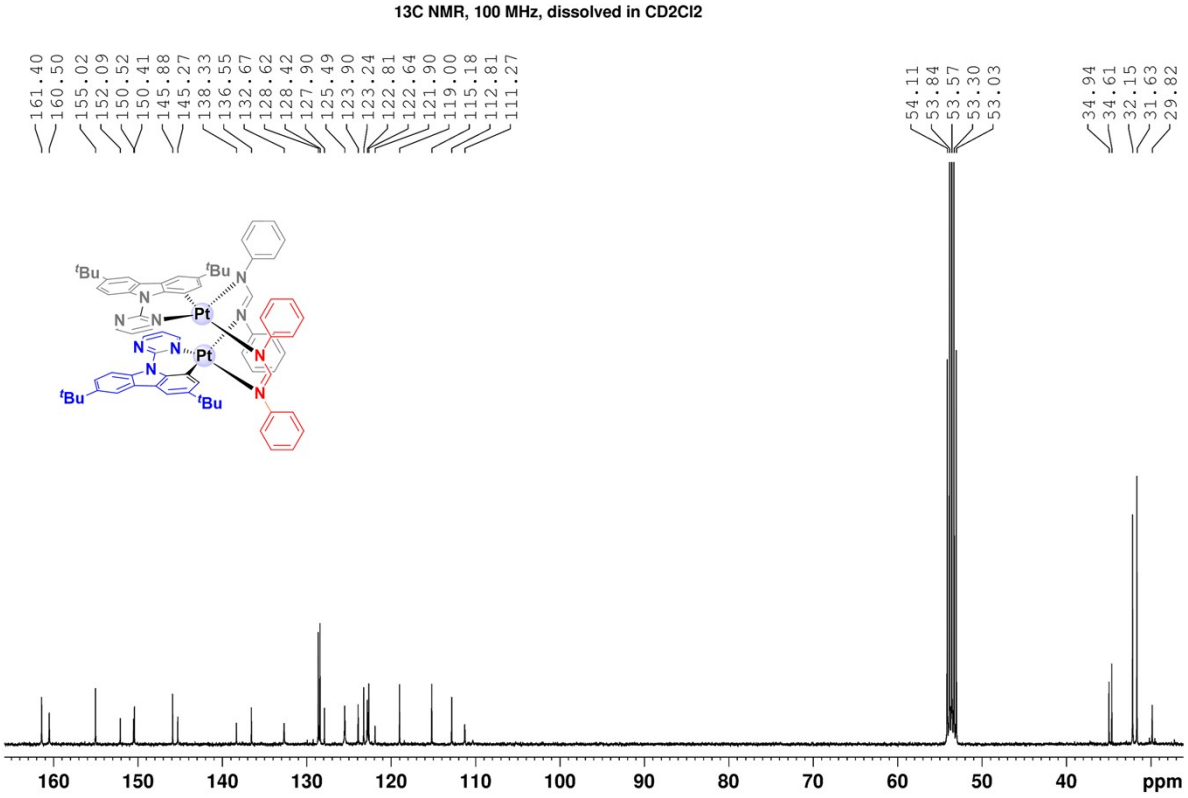

Figure S23. ^{13}C NMR spectrum of **1-*anti*** (CD_2Cl_2)

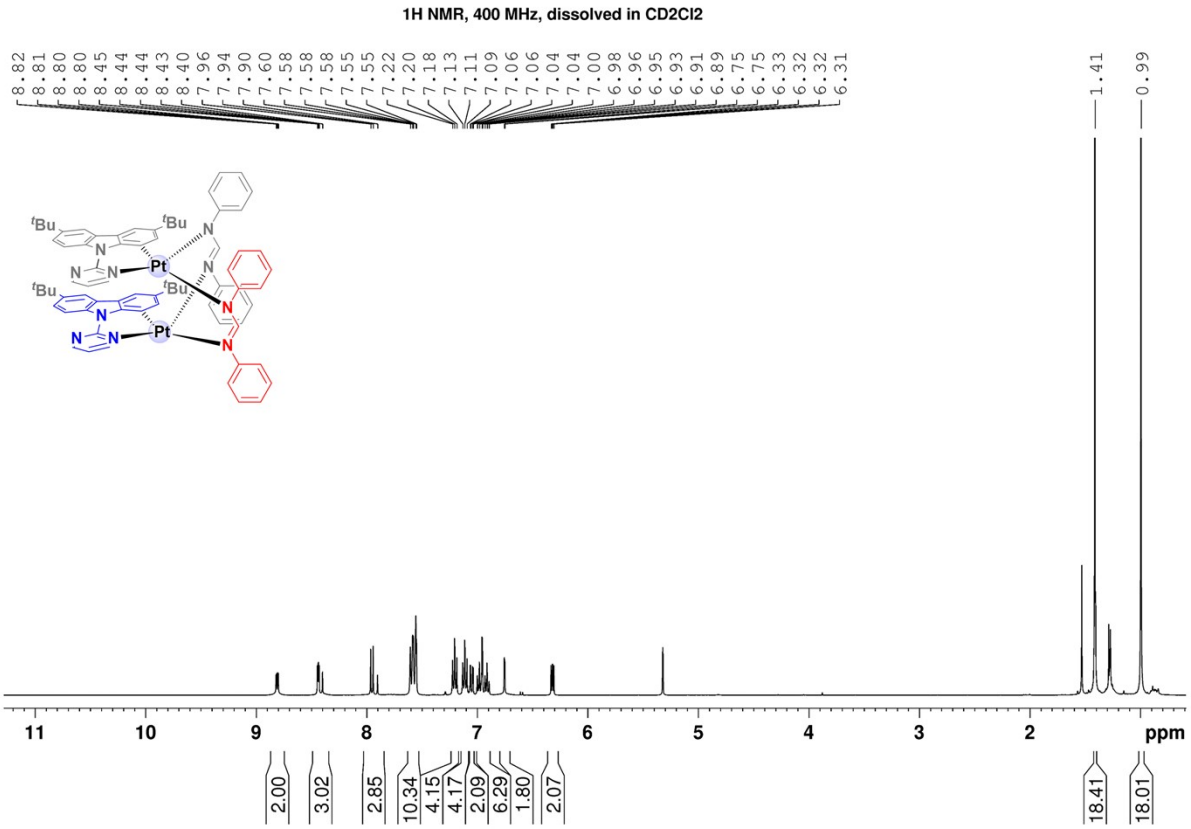

Figure S24. ^{1}H NMR spectrum of **1-*syn*** (CD_2Cl_2)

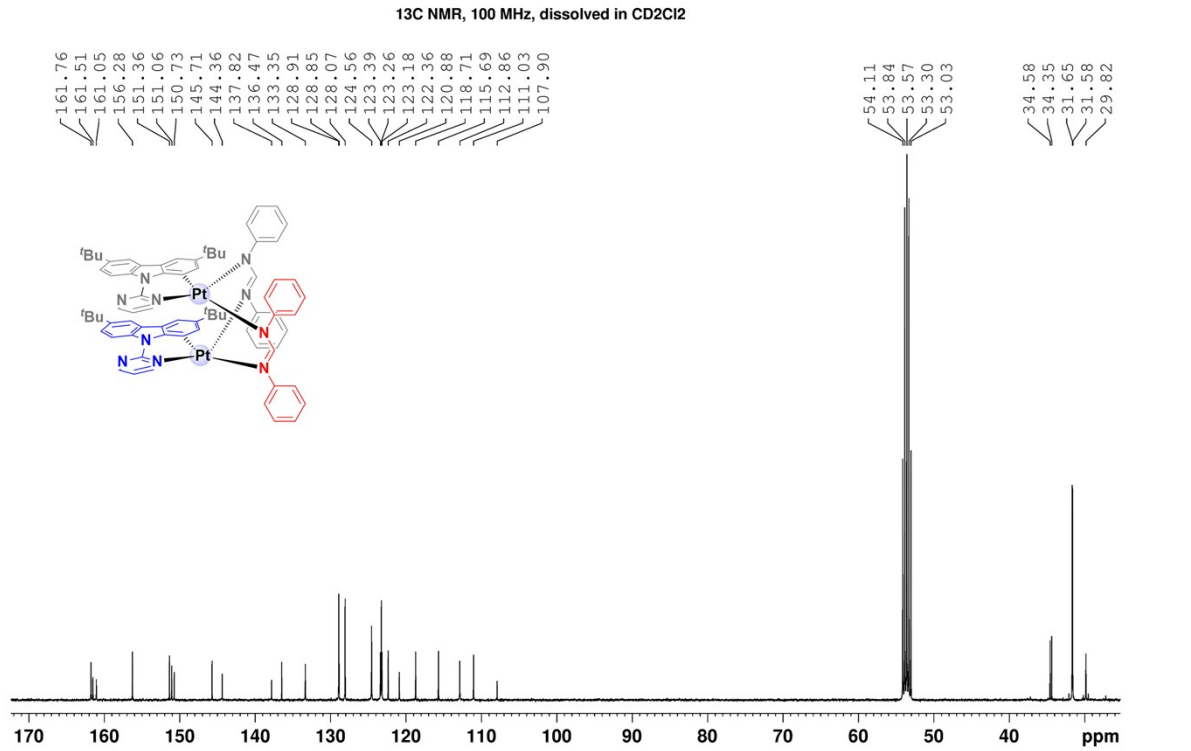

Figure S25. ^{13}C NMR spectrum of **1-*syn*** (CD_2Cl_2)

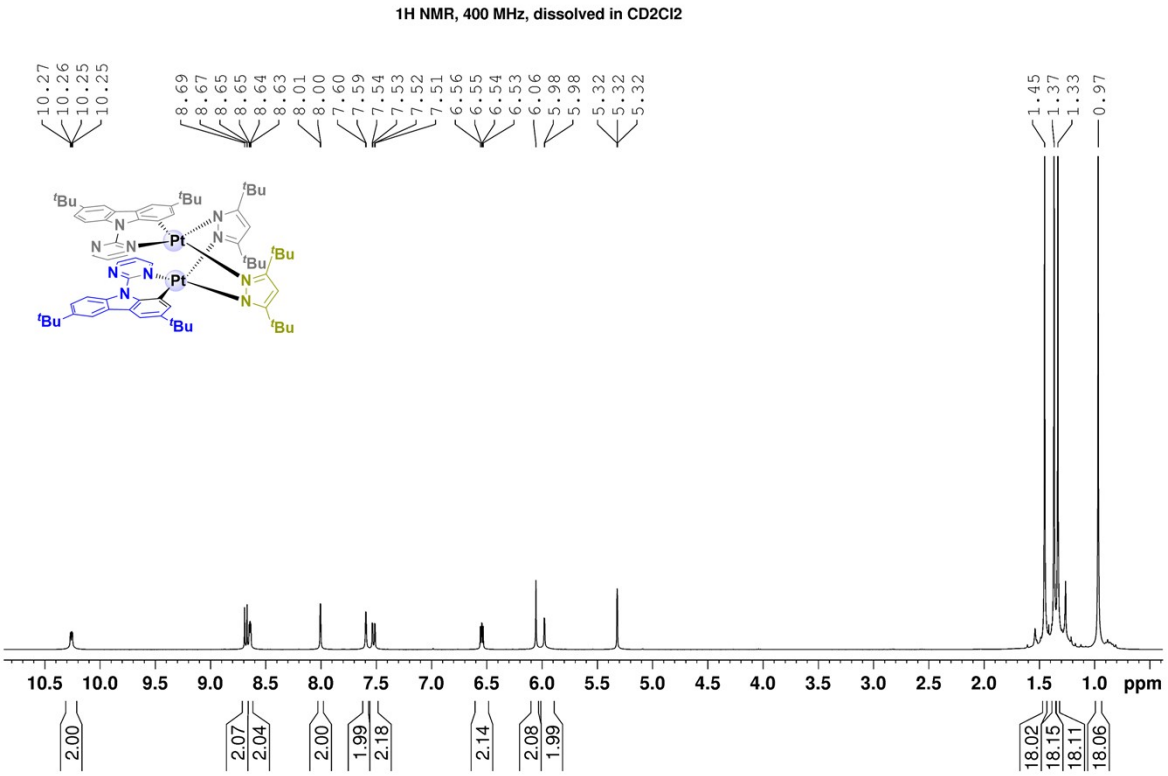

Figure S26. ^{1}H NMR spectrum of **2-*anti*** (CD_2Cl_2)

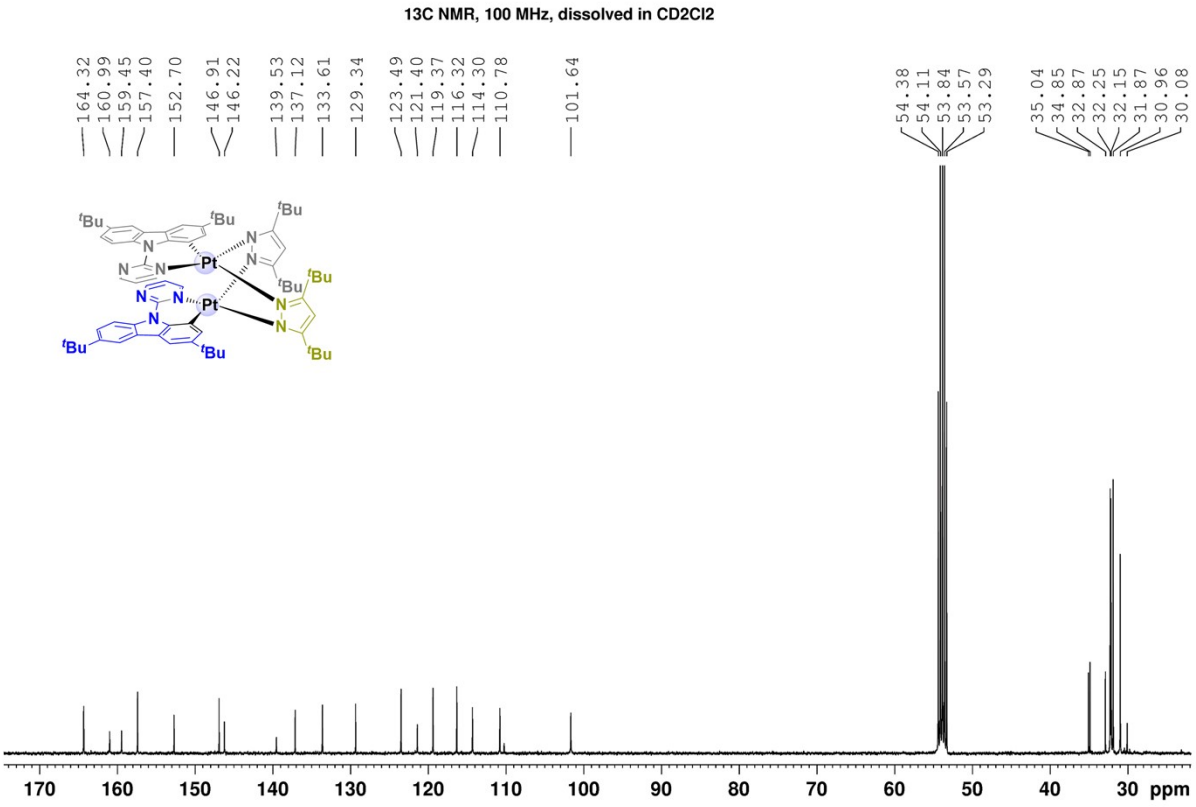

Figure S27. ^{13}C NMR spectrum of **2-*anti*** (CD_2Cl_2)

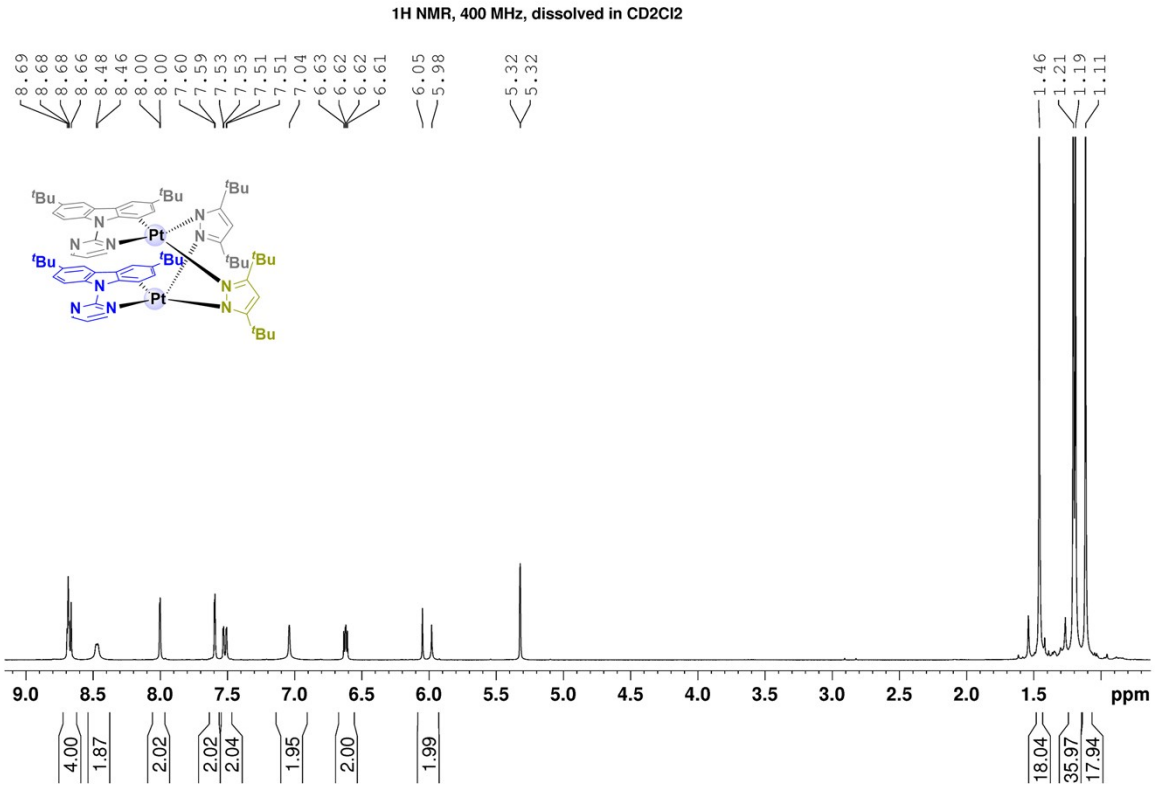

Figure S28. ^{1}H NMR spectrum of **2-*syn*** (CD_2Cl_2)

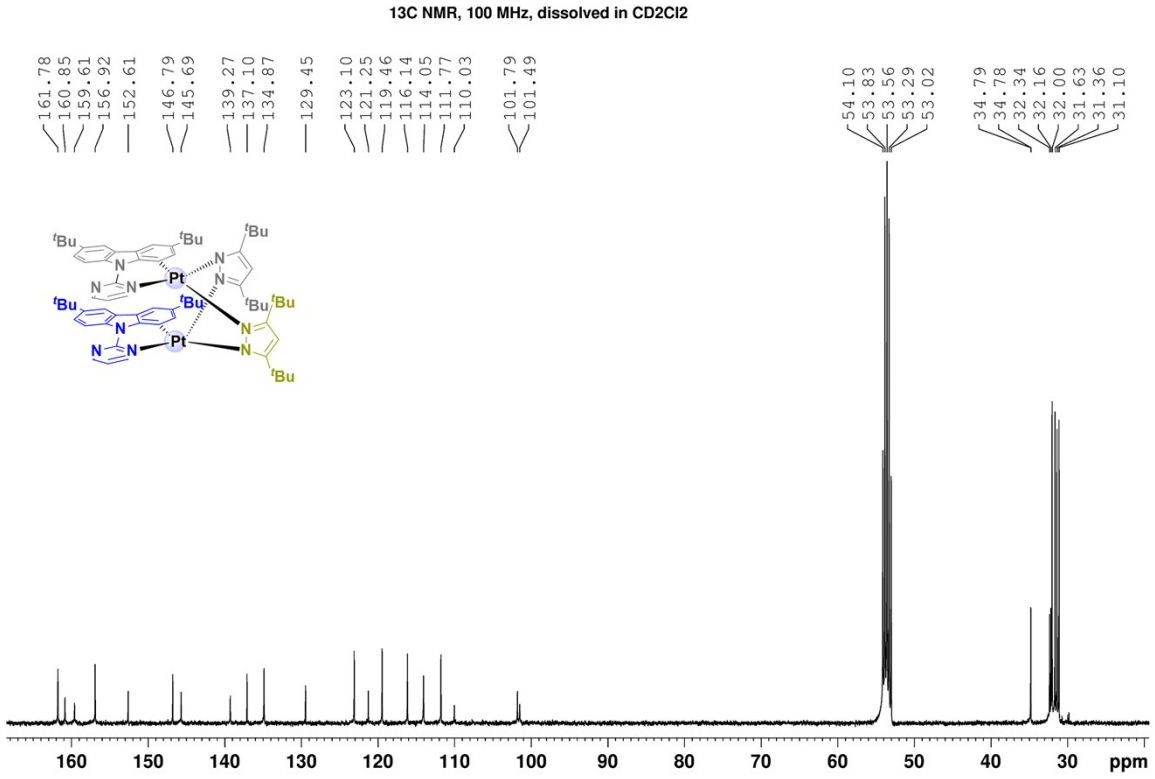

Figure S29. ^{13}C NMR spectrum of **2-*syn*** (CD_2Cl_2)

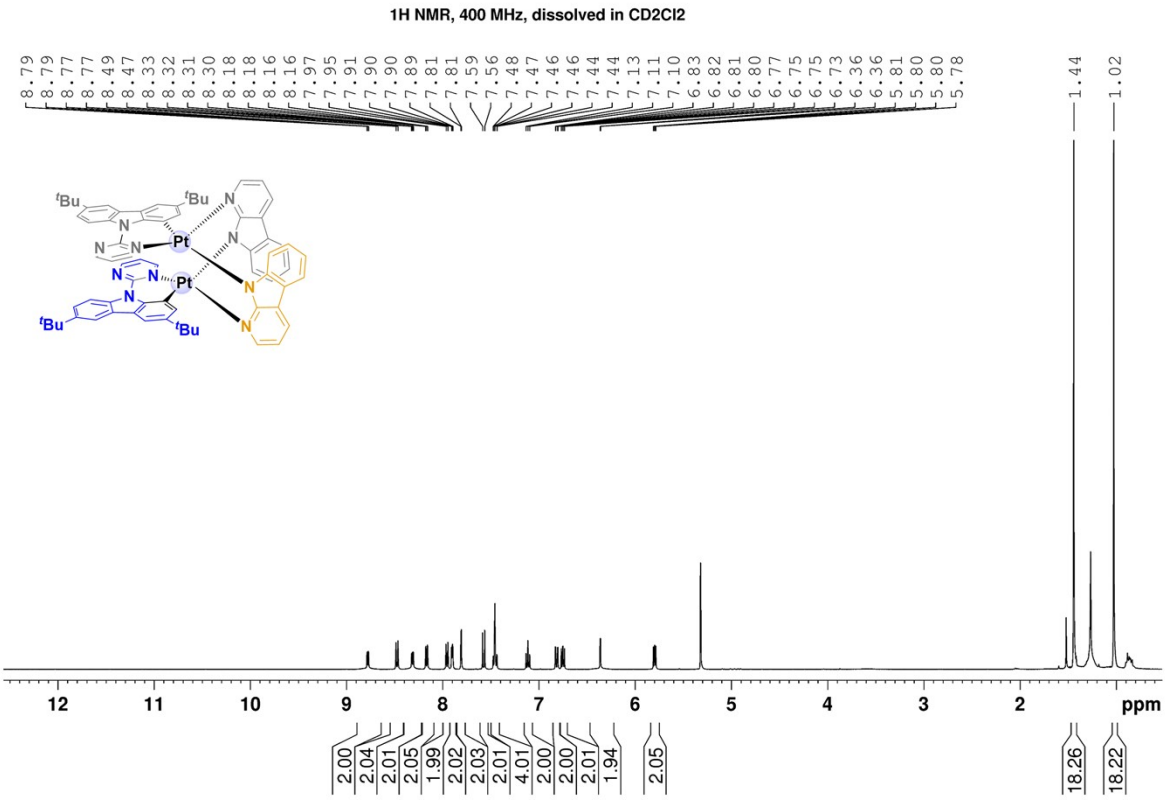

Figure S30. ^{1}H NMR spectrum of **3** (CD_2Cl_2).

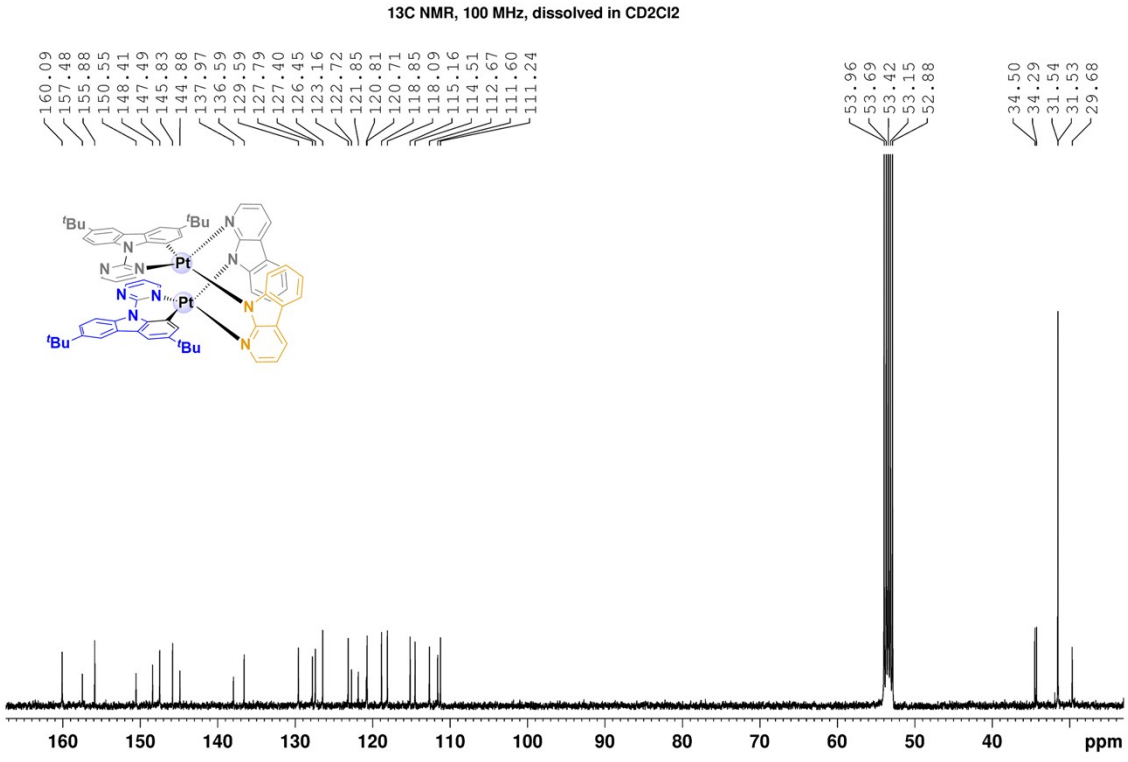

Figure S31. ^{13}C NMR spectrum of **3** (CD_2Cl_2)

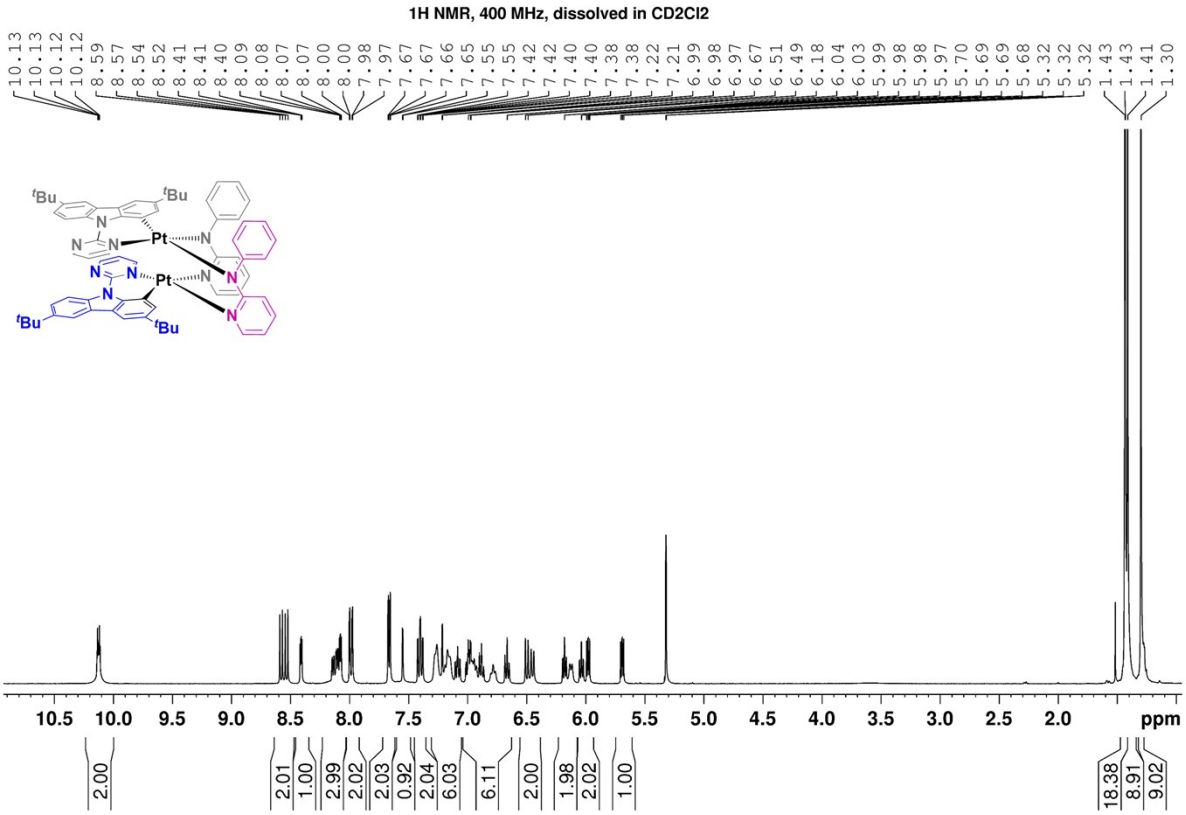

Figure S32. ^{1}H NMR spectrum of **4** (CD_2Cl_2).

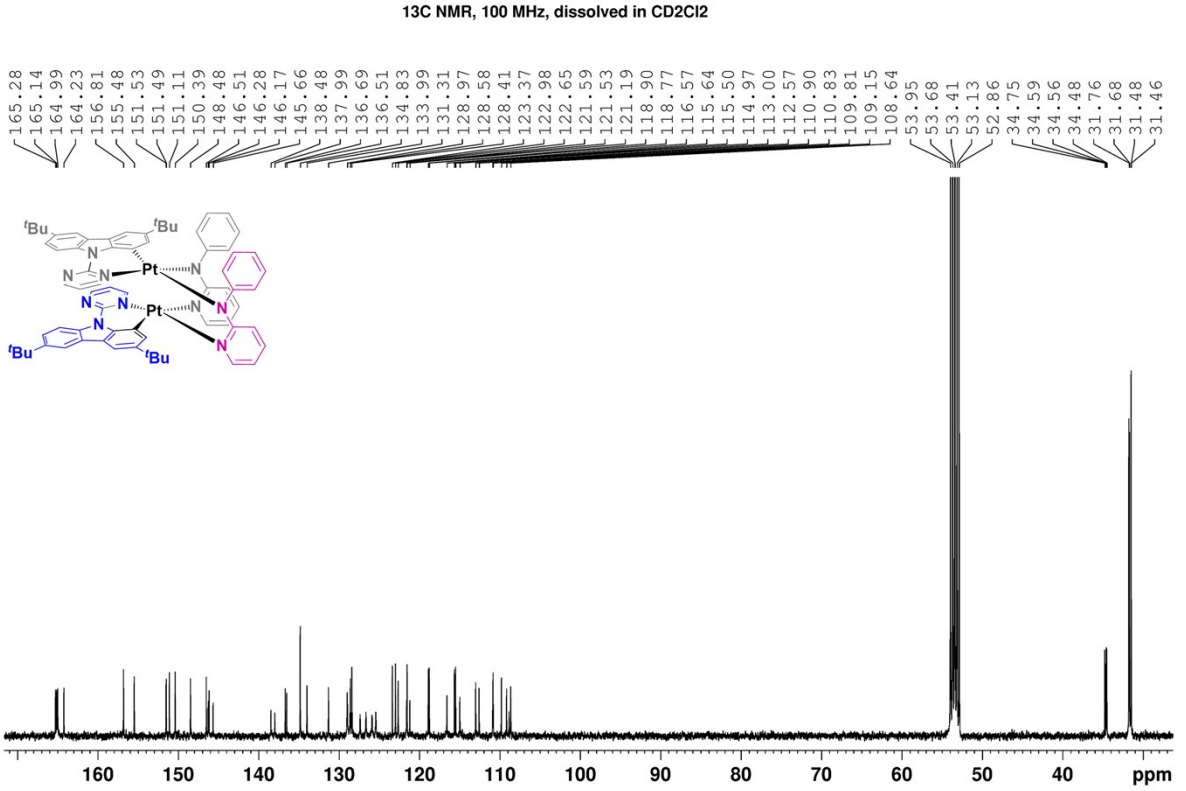

Figure S33. ^{13}C NMR spectrum of **4** (CD_2Cl_2)

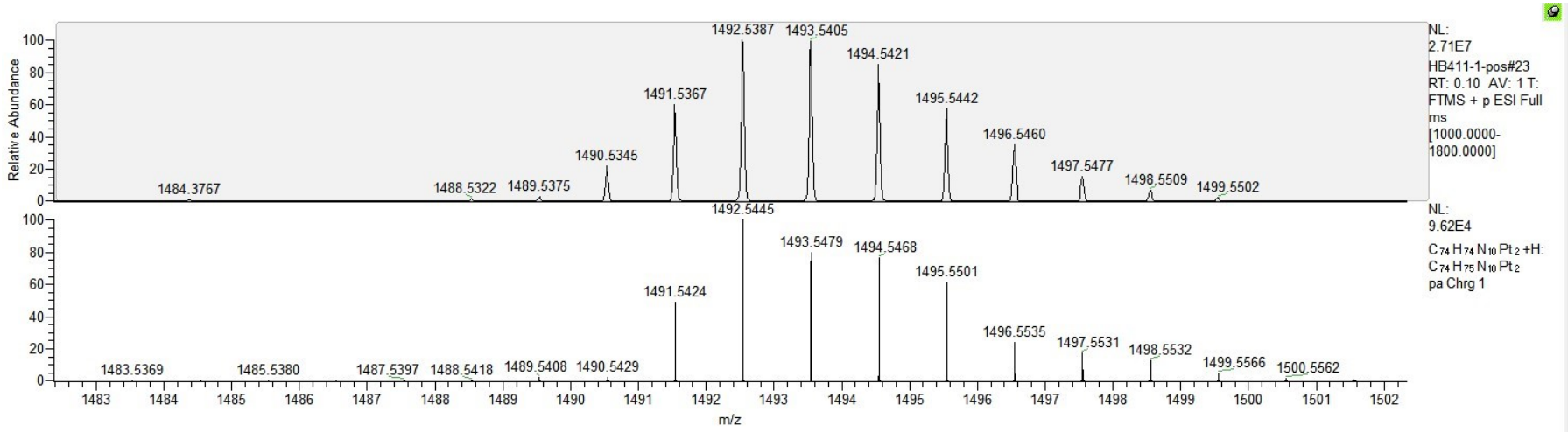

Figure S34. HRMS spectra for **1-*anti*** [M + H]$^+$.

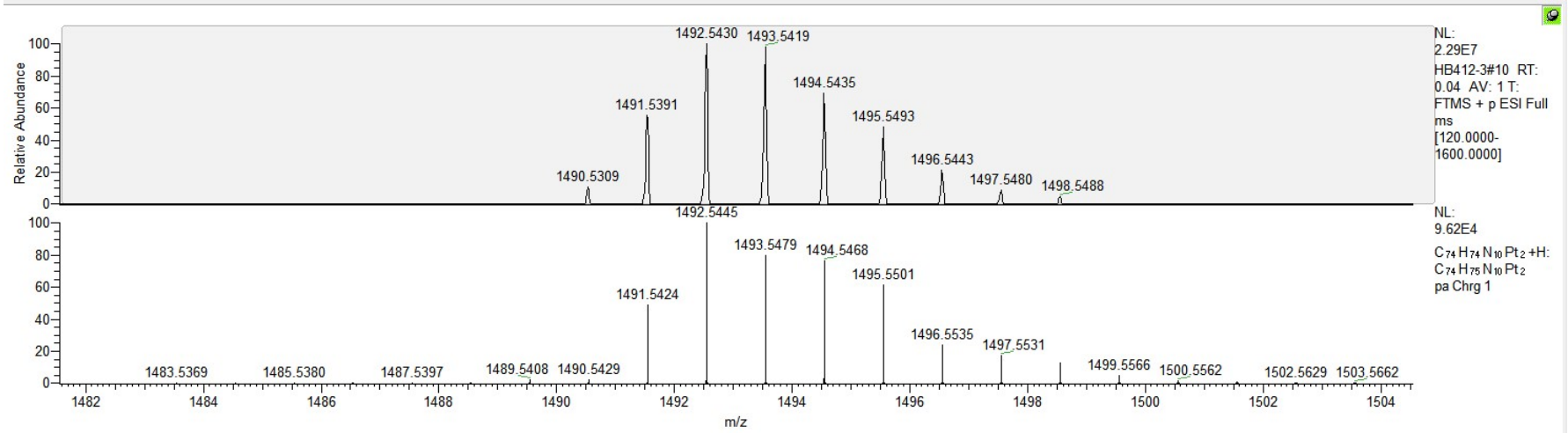

Figure S35. HRMS spectra for **1-*syn*** [M + H]$^+$.

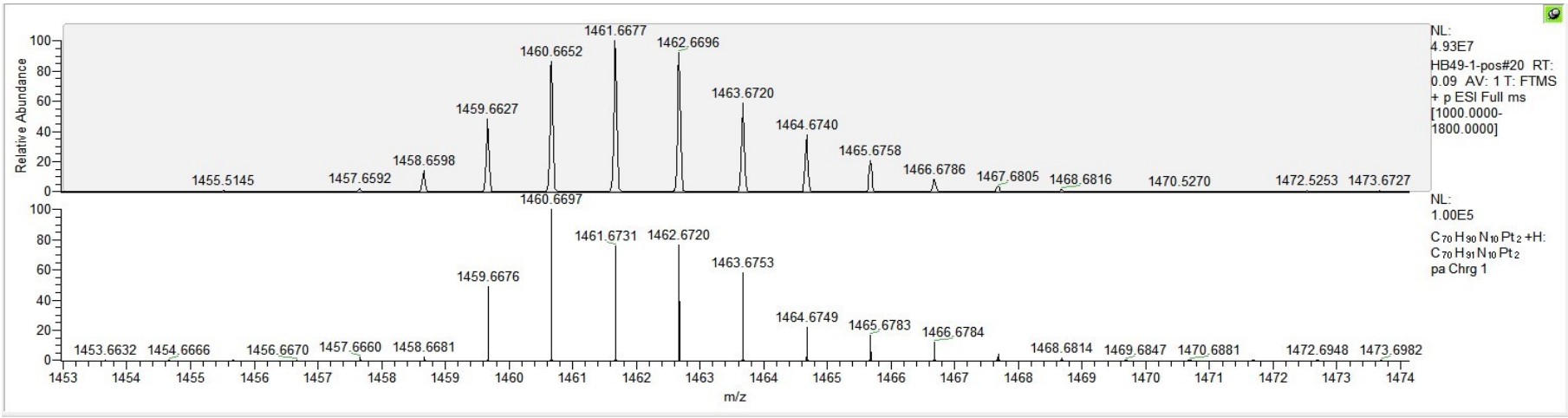

Figure S36. HRMS spectra for **2-*anti*** $[M + H]^+$.

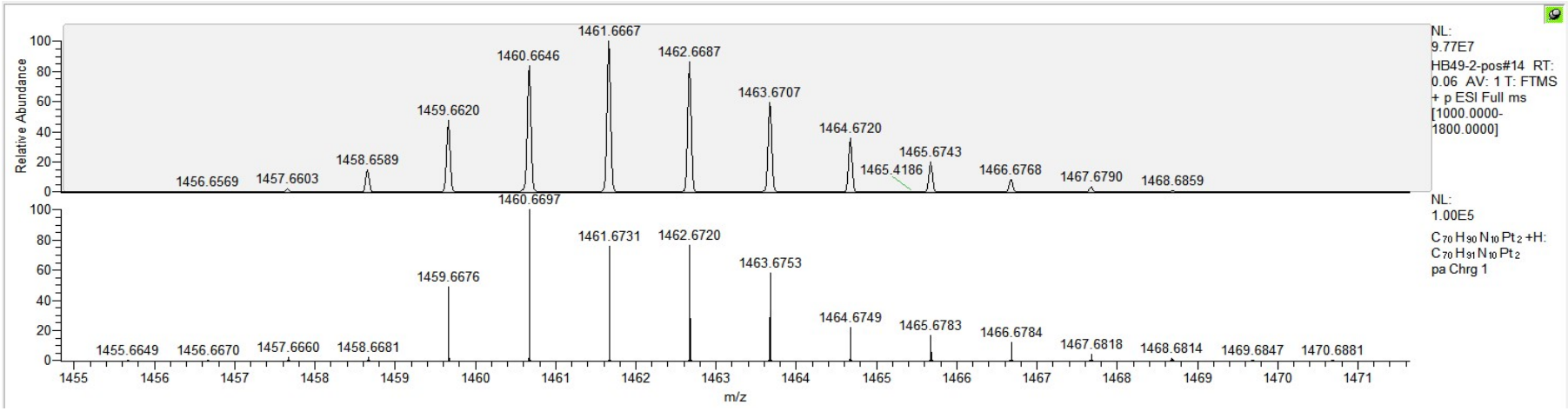

Figure S37. HRMS spectra for **2-*syn*** $[M + H]^+$.

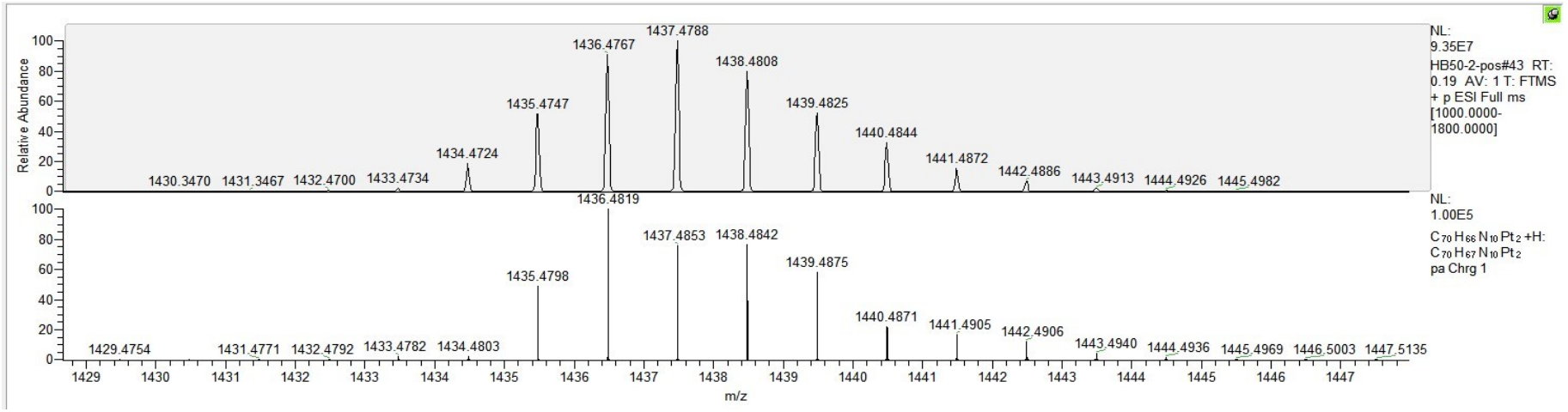

Figure S38. HRMS spectra for **3** $[M + H]^+$.

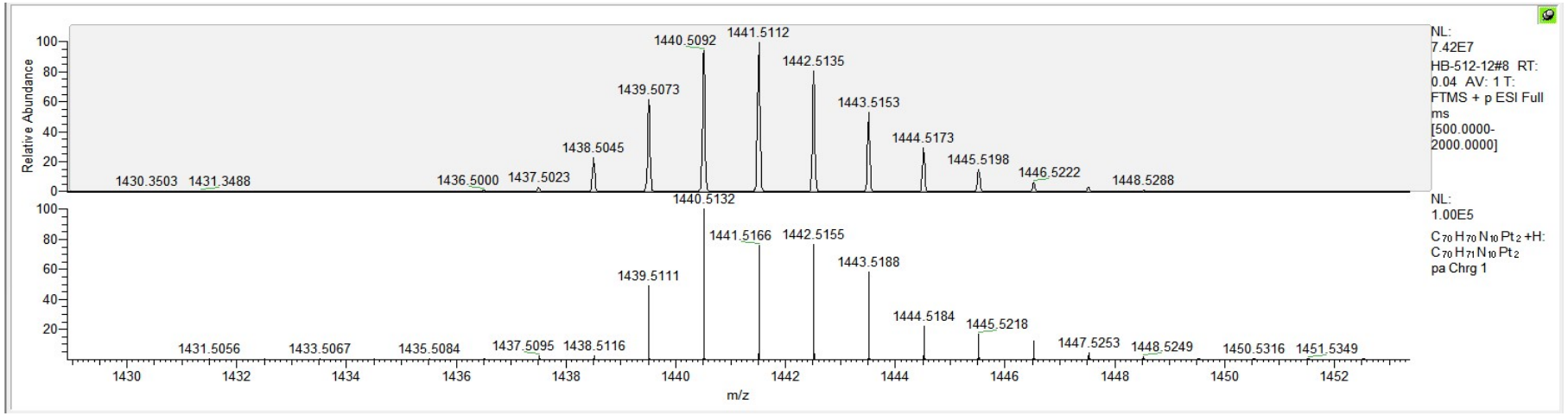

Figure S39. HRMS spectra for **4** $[M + H]^+$